What can go wrong in a dividing wall column and how to detect it

Lena-Marie Ränger[1,2], Ivar J. Halvorsen[1], Thomas Grützner[2], Sigurd Skogestad*[1]

[1]Department of Chemical Engineering, Norwegian University of Science and Technology, Trondheim, Norway

[2]Laboratory of Thermal Process Engineering, Institute of Chemical Engineering, Ulm University, Ulm, Germany

*Corresponding author, sigurd.skogestad@ntnu.no

Abstract

Dividing wall columns are state-of the art distillation arrangements performing three separation tasks within one unit. Compared to using two conventional columns in series this saves both capital costs and energy but on the other hand it brings a higher risk of malfunction. This simulation study analyses what can go wrong during the operation of dividing wall columns. The emphasis is on the operation of the prefractionator section, that is, on the choice on the liquid and vapor splits, which is crucial for the overall performance. The resulting two-way flows between the prefractionator and main column gives a broader feasible operating range than in a conventional column arrangement. This can lead to peculiar behavior, including circulation of components around the dividing wall. This paper identifies 15 non-optimal operating regions for the prefractionator with specific internal flow patterns, characteristic temperature and composition profiles for the separation of a fairly ideal mixture of benzene, toluene and *p*-xylene. From these results it is possible to identify and hopefully rectify wrong choices for the liquid and vapor splits in a dividing wall column.

Keywords

Distillation, Petlyuk column, energy savings, integrated design, intensified units, liquid split ratio, vapor split ratio, malfunction, simulation

1 Introduction

Dividing wall columns (Figure 1a) are intensified distillation arrangements that typically can save around 30 % or more, both in terms of energy consumption and capital costs, compared to conventional distillation columns [1–5]. They are a thermally and materially coupled version of a conventional three-column arrangement with a prefractionator. Consider the separation of three components (A, B and C). The light and heavy components (A and C) are separated in the prefractionator (marked green in Figure 1a), while the intermediate (middle boiling) component (B) distributes to both products of the prefractionator. The resulting two binary product streams (AB in the top and BC in the bottom of the prefractionator) are fed at different locations into the main column (marked red and yellow in Figure 1a) to finalize the separation, with component A in the top (distillate) product, B in the side product and C in the bottom's product. The upper main column (red) separates A and B and the lower main column (yellow) separates B and C [6–8].

In order to achieve pure products from a dividing wall column, not only must one ensure that enough energy is provided to the main column, but it is also crucial that the prefractionator performs a sharp split between A and C. This can only be guaranteed, if the liquid and vapor recycle streams to the prefractionator (as given by the split ratios R_L and R_V) are properly set. Fortunately, because of the flexibility in the distribution of the intermediate component B, these flows do not have to be at a specific value but within a certain range, which is denoted as the optimality region. In real plants the liquid split R_L is fairly easy to manipulate. However, the vapor split R_V is usually not manipulated but instead set by careful column design [9].

Many publications focus on the optimal design and operation of dividing wall columns [10–14]. However, during operation, for example due to disturbances in the feed flow, feed composition, or feed state (liquid fraction), it can easily happen that one or both of the split ratios end up outside the optimal range, which generally makes it impossible to achieve the desired sharp separation at minimum energy consumption. The authors are not aware of a publication that evaluates the consequences of a non-optimal operation of the prefractionator. Correspondingly, the objective of this contribution is to close this gap and investigate how wrong operation of the prefractionator, that is, non-optimal values for the liquid and vapor splits (R_L and R_V), affects the internal component flows and product compositions in a dividing wall column.

An extensive case study is performed for a ternary, equimolar and close to ideal mixture of A = Benzene, B = Toluene and C = *p*-Xylene (BTX for short). The feed is in the liquid saturated state, and all three products of the main column, including the side product, are assumed to be in the liquid state. Additionally, in all simulations a high number of theoretical stages is assumed so that pinch zones are visible. Finally, to simplify the analysis, it is assumed that the three product

flows from the main column are fixed at the flow of the corresponding target components (A, B or C) in the feed. Since the feed is assumed to be equimolar, this means that in all simulations the main column product flows are $\dot{D}_{C11} = \dot{S} = \dot{B}_{C14} = \dot{F}/3$. It would also be possible to make other assumptions for the main column, for example, that the top and bottom products $\left(\dot{D}_{C11} \text{ and } \dot{B}_{C14}\right)$ are (almost) pure, but the main emphasis in this paper is on the prefractionator, and it is believed that the effect of the main column operation is limited.

The paper is structured as follows. First, Section 2 summarizes the theoretical background, including an in-depth discussion on how the temperature profile should look like during proper operation. Then, Section 3 summarizes the methodology used for the simulation case study. In Section 4, results are presented, which includes a classification of feasible non-optimal scenarios and their detection using temperature profiles. These results were derived for the above mentioned rather ideal BTX mixture and the results may be different for non-ideal mixtures or for other ways of operating the main column. Correspondingly, Section 5 comments on the generalization of the results. Last, conclusions are drawn in Section 6.

2 Theoretical Background

This Section summarizes the most important theoretical background, starting with the dividing wall columns itself (Section 2.1). Next, the focus is on $\dot{V}_{\min}$ diagrams and their application to dividing wall columns (Section 2.2). This includes a discussion on the theoretically optimal operation of dividing wall columns with side condenser or side evaporator (Section 2.2.1), the optimality region resulting for typical three-product dividing wall columns without side condenser/evaporator (Section 2.2.2) and the operational flexibility resulting when allowing impurities in the products or providing more energy than the minimum (Section 2.2.3). Last, to understand the corresponding resulting composition and temperature profiles, Subsection 2.3 briefly summarizes relevant information on pinch zones.

2.1 Dividing wall columns

Figure 1a shows a dividing-wall column with six sections, a dividing wall and three products, including a side product. Figure 1b shows the corresponding thermodynamically equivalent Petlyuk sequence consisting of three subcolumns. In Figure 1c, the optimal paths of the three components (A, B, C) through the dividing wall column are visualized.

Sections C21 and C22 (green), which make up the prefractionator, are meant to separate components A and C, while component B distributes. Sections C11 to C14, known as the main column, act as two separate columns on top of each other, each with a binary feed. Sections C11

and C12 (red) separate components A and B, whereas sections C13 and C14 (yellow) separate components B and C [6–8].

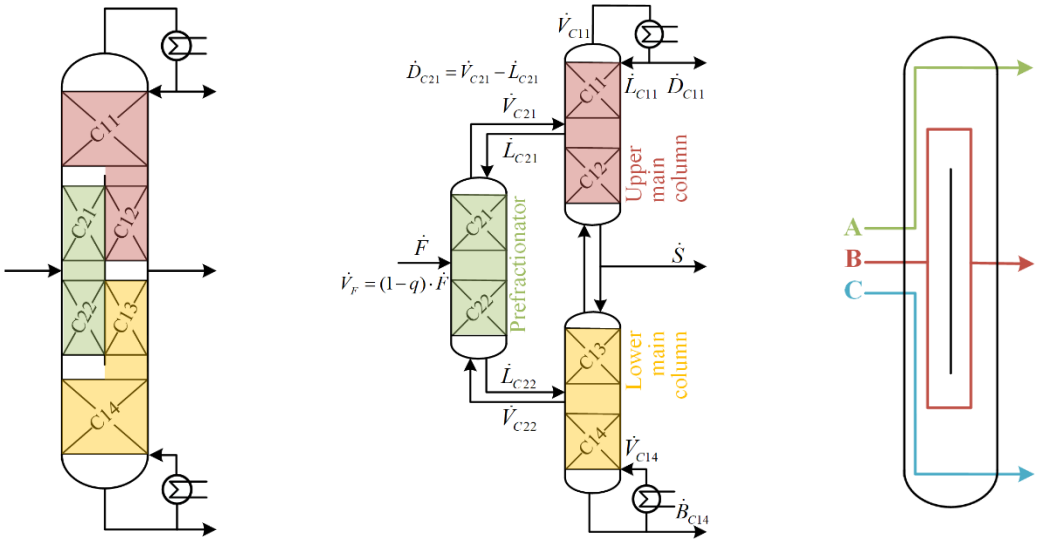

Figure 1: (a) Dividing wall column arrangement with subcolumns indicated by different colors, (b) corresponding Petlyuk sequence with flow nomenclature. All physical flows are assumed non-negative. (c) Optimal net flow paths of three components through the dividing wall column (see Equation (16)).

The three product flows in Figure 1b must be positive at steady state:

$$\dot{D}_{C11} \geq 0, \;\; \dot{S} \geq 0, \;\; \dot{B}_{C14} \geq 0 \tag{1}$$

and they must also satisfy the overall steady-state mass balance

$$\dot{F} = \dot{D}_{C11} + \dot{S} + \dot{B}_{C14} \tag{2}.$$

For sharp separations, the product flows must equal the fractions of the components in the feed z_i. times the absolute feed flow $\dot{F}$.

$$\begin{aligned} \dot{D}_{C11} &= z_A \cdot \dot{F} \\ \dot{S} &= z_B \cdot \dot{F} \\ \dot{B} &= z_C \cdot \dot{F} \end{aligned} \tag{3}$$

and this has been assumed in the simulations in this paper, also for non-sharp separations. The distillate flows for the main column and the prefractionator are

$$\dot{D}_{C11} = \dot{V}_{C11} - \dot{L}_{C11} \tag{4}$$

$$\dot{D}_{C21} = \dot{V}_{C21} - \dot{L}_{C21} \tag{5}$$

As stated in Equation (1), the distillate product from the main column is a physical flow, and it is required that $\dot{D}_{C11} \geq 0$. Correspondingly, for the upper part of the main column C11, the flow constraints are:

$$\dot{V}_{C11} \geq 0,\ \dot{L}_{C11} \geq 0,\ \dot{V}_{C11} \geq \dot{L}_{C11} \tag{6}$$

On the other hand, the prefractionator section C21 does not have a physical distillate product stream, so $\dot{D}_{C21}$ is the net flow resulting from the difference between the vapor and liquid flows. The only constraints that have to be fulfilled here are that

$$\dot{V}_{C21} \geq 0,\ \dot{L}_{C21} \geq 0 \tag{7},$$

so it may happen that $\dot{D}_{C21}$ becomes negative.

Here, by introducing the feed vapor flow

$$\dot{V}_F = (1-q) \cdot \dot{F} \tag{8},$$

where q is the liquid fraction in the feed, and assuming constant molar flows, the vapor flows at the top of the main column and prefractionator become

$$\dot{V}_{C11} = \dot{V}_F + \dot{V}_{C14} \tag{9}$$

$$\dot{V}_{C21} = \dot{V}_F + \dot{V}_{C22} \tag{10}.$$

Two important operating parameters of the dividing wall column are the vapor and liquid split ratios from the main column to the prefractionator [15]. These are defined as recycle flows to the prefractionator divided by the corresponding total flow in the main column (see Figure 1a):

$$R_V = \frac{\dot{V}_{C22}}{\dot{V}_{C14}} = \frac{\dot{V}_{C21} - \dot{V}_F}{\dot{V}_{C14}} \tag{11}$$

$$R_L = \frac{\dot{L}_{C21}}{\dot{L}_{C11}} = \frac{\dot{V}_{C21} - \dot{D}_{C21}}{\dot{V}_{C14} + \dot{V}_F - \dot{D}_{C11}} \tag{12}$$

Both R_L and R_V are between 0 and 1. The expression for R_L in Equation (12) in terms of vapor flows is useful for the later analysis using the $\dot{V}_{\min}$ diagram. The expression assumes constant molar flows, which does not exactly hold in the simulations, but the error is small for the simulated BTX-mixture.

As mentioned, the dividing wall column is a thermally and materially coupled version of three conventional columns; a prefractionator column for the AB-BC split, a second column for the A-B split and a third column for the B-C split. A conventional two-product distillation column with a given feed has five design variables at steady state, which are the number of stages above and below the feed stream (N and N_F), the pressure (p) and two specifications (e.g., reflux and boilup,

or heating and cooling, or reflux and distillate flow) that determine the compositions of the two product streams. So, a combination of three columns theoretically have 15 design variables. However, for the dividing wall arrangements, the pressures are the same which gives two less, and the top product of C13+C14 is combined with the bottom product of C11+C12 to make only one side product (S). This further reduces number by one, resulting in 12 design variables for a dividing-wall column with a given feed (for example, the pressure, the number of stages in 6 sections, the distillate flow $\dot{D}_{C11}$, the boilup $\dot{V}_{C14}$, the side stream flow $\dot{S}$ and the two internal splits, R_l and R_v) [16]. In order to optimally design such columns, rigorous and shortcut methods are available [14,17], the detailed explanation of which exceeds the scope of this work. A very useful tool to visualize the internal flows required for the separation is the $\dot{V}_{\min}$ diagram [18], which is explained shortly in the following Section 2.2. For more detailed information regarding their calculation, the reader is referred to literature [19–22].

2.2 The $\dot{V}_{\min}$ diagram and its application to dividing wall columns

Assume that the pressure is given. Then, at infinite number of stages, there are just two degrees of freedom left to determine the operating point of a conventional two-product distillation column. In the minimum vapor demand ($\dot{V}_{\min}$) diagram, the independent variable is chosen as the distillate flow $\dot{D}$ in ratio to the fed stream $\dot{F}$. The diagram displays the resulting vapor flow ($\dot{V}_{\min}/\dot{F}$), which is a "mountain" curve giving the minimum vapor flow required for sharp separation with an infinite number of stages for a given distillate flow (black lines in Figure 2a). In addition, various feasible operating regions can be identified in the diagram, as discussed in detail in this paper.

The diagram can be calculated for any feed mixture with an arbitrary number of components *k*, either in a simplified (ideal) way by assuming constant relative volatility and constant molar flows (using the Underwood equations) or rigorously using flowsheet simulations [19]. The resulting mountain curve for $\dot{V}_{\min}/\dot{F}$ has *k*-1 maximum points and $k\cdot(k-1)/2$ minima in between [18,19]. Each point represents $\dot{V}_{\min}/\dot{F}$ for a sharp split between all possible selected pair of keys. E.g.:with a 4-component feed (ABCD) the top peaks represent sharp splits: A-BCD, AB-CD and ABC-D. The next row is when one component is distributed: AB-BCD and ABC-CD, and finally the preferred split ABC-BCD where B and C distribute to both ends. The curves between these points are distribution boundaries where a certain component is at the boundary of becoming distributed to both ends or disappear from one end for a slight increase or decrease in vapor rate. These curves are straight lines in the ideal case of constant relative volatilities and constant molar flows. If these assumptions do not hold, the boundary lines may be slightly curved. The maxima represent the minimum energy requirement for sharp separation between products, where each component is only present in one of the product streams. The curve in between represents minimum energy

operation with some components distributing between the product streams, while the other components are found in only one product stream. If a column is operated in the region above the $\dot{V}_{\min}$ curve ("overpurified"), more energy is used than needed. On the other hand, if less vapor is provided ("underpurified"), additional components start to distribute, that is, the separation is no longer sharp.

In the context of $\dot{V}_{\min}$ diagrams, often the term recovery is used, which is defined as

$$r_i^{top} = \frac{x_i^D \cdot \dot{D}}{x_i^F \cdot \dot{F}} \tag{13}$$

$$r_i^{bot} = \frac{x_i^B \cdot \dot{B}}{x_i^F \cdot \dot{F}} = 1 - r_i^{top} \tag{14}.$$

Here *top* refers to the top end of the column and *bot* to the bottom end. x_i is the molar fraction in the feed stream of component *i*.

The $\dot{V}_{\min}$ diagram is also useful for a dividing wall column. Interestingly, the minimum energy demand for this complex arrangement is represented by the highest peak in the $\dot{V}_{\min}$ diagram. More details on how to optimally operate the dividing wall column, including determining from the $\dot{V}_{\min}$ diagram a suitable operating point/range for the prefractionator, are given in the following Subsections: Subsection 2.2.1 focuses on the "perfect" operation of a dividing wall column, in which all three subcolumns are operated at their minimum energy demand. This "perfect" operation either happens in the unlikely case that the A-BC and AB-C separations require exactly the same amount of vapor, or in the (fairly common) case that the column has a side condenser/evaporator at the side draw stage. This scenario is of interest as it results in composition and temperature profiles which are not distorted by remixing effects. However, a typical three-product dividing wall column does not have a side condenser/evaporator. Then, the easier of the two separations (A-B or B-C) in the main column is overpurified. Consequently, the prefractionator itself does not need to be operated exactly at its minimum energy (which occurs at *the preferred split*) but can be operated in the range between the preferred and balanced splits, which is the so-called optimality region (Subsection 2.2.2). If additional impurities are allowed in the products or if more than the minimum energy demand is provided in the main column, the optimality region broadens to a flexibility region, which is described in more detail in Subsection 2.2.3.

Note that the $\dot{V}_{\min}$ diagram is originally only valid at an infinite number of stages, thus minimum energy demand. However, it has been shown that it can be extended to lower numbers of stages with higher energy demand [23]. The visualization is still very useful to understand for which energy input which component distribution can be expected. As stated before, the results in this

article are obtained for a high number of stages, but due to the concept of the stage-adapted $\dot{V}_{min}$ diagram it can be assumed that the results can be transferred to a lower number of stages.

2.2.1 "Perfect" operation of a dividing wall column without remixing effects

Figure 2 illustrates the "perfect" operation (denoted with the letter a) of a dividing wall column without remixing effects: the upper part of the main column is operated at the A-BC peak (labeled C11+C12 a), the lower part of the main column at the AB-C peak (C13+C14 a) and the prefractionator at the AB-BC minimum which is called the *preferred split* (C21+C22 a). Operating the prefractionator at the preferred split means that it is operating at the minimum energy demand and components A and C are both at the limit to be distributing to its top and bottom product (lines with $r_A^{bot} = 0$ and $r_C^{top} = 0$ in Figure 2). The resulting composition and temperature profile for this "perfect" operation of a dividing wall column is evaluated in Section 4.1 (results).

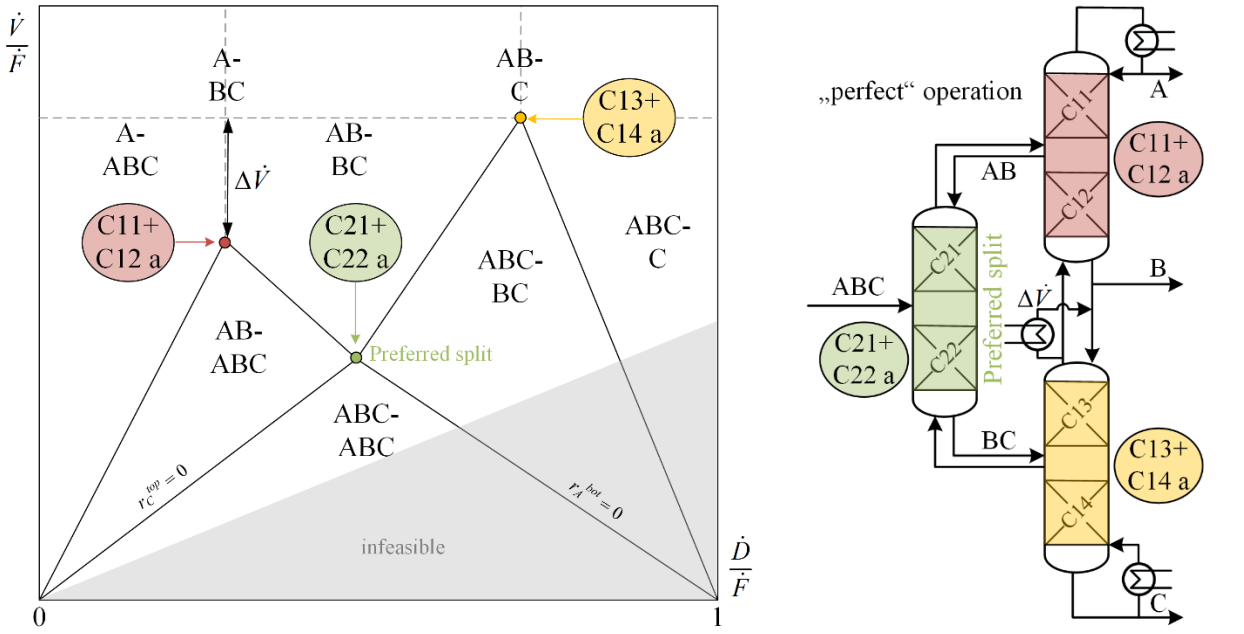

Figure 2: (a) $\dot{V}_{min}$ diagram (black solid lines) valid for a conventional two-product distillation column or a Petlyuk sequence (equivalent to a dividing wall column) for the BTX mixture. (b) Flowsheet for the case with "perfect" operation of the three Petlyuk subcolumns by making use of a side condenser with cooling duty $\Delta\dot{V}$. Notation: Components obtained in the top product of a (sub-) column are given before the hyphen and components in the bottom product behind the hyphen.

2.2.2 The optimality region

Usually dividing wall columns do not have a side condenser/evaporator (Figure 3b). The vapor requirement in the main column is then the one of the more difficult split, that is, equal to the highest peak in the $\dot{V}_{min}$ diagram. In this case, if the prefractionator is operated at the *preferred*

split, then the easier split in the main column, the one with the lower peak, is performed with excess vapor. This results in overpurification of the product in the corresponding section in the main column (the top product for the BTX-case in Figure 3a). Temperature and composition profiles for a dividing wall column operated at minimum energy consumption and the prefractionator at the preferred split are shown in Section 4.2.1 (results).

Alternatively, by changing the liquid or vapor split, the excess vapor may be used to give overpurification in the prefractionator. The extreme is the so-called *balanced split* (point C21+C22 b in Figure 3a), where all the excess vapor that could be removed in a side condenser (or excess liquid for a side heater) is sent to the prefractionator. Then, the lower section of the prefractionator is overpurified and the fraction of A in the bottom becomes even smaller. Temperature and composition profiles for a dividing wall column operated at minimum energy consumption and the prefractionator at the balanced split are shown in Section 4.2.2 (results).

Thus, minimum energy operation of the overall dividing wall column $\left(\dot{V}_{C14} = \max\left(\dot{V}_{\min}^{A-BC}, \dot{V}_{\min}^{AB-C}\right)\right)$ may be achieved with the prefractionator operating within an *optimality region* between the preferred split and the balanced split (represented by the thin green thick line in Figure 3a). [20]

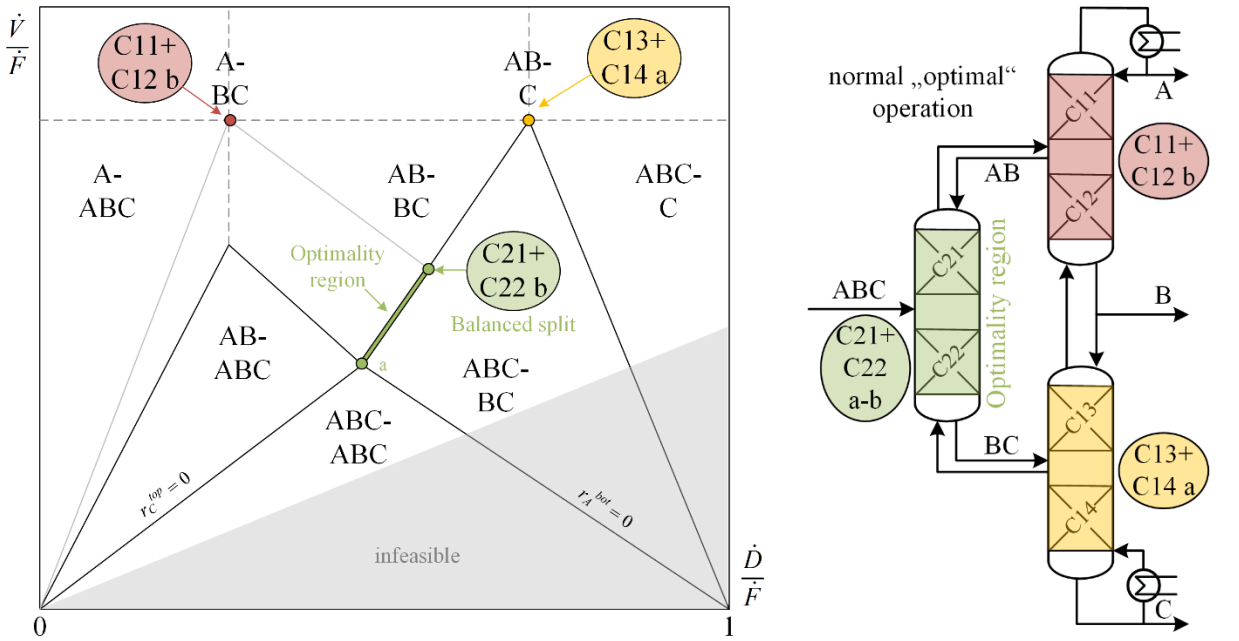

(a) (b)

Figure 3: (a) $\dot{V}_{\min}$ diagram (black solid lines) for the BTX mixture for the typical three-product dividing wall column in (b), without a side condenser. Components obtained in the top product of a (sub-) column are given before the hyphen and components in the bottom product behind the hyphen. Minimum energy operation may be obtained with the prefractionator operating within the "optimality region" between the preferred split (point (C21+C22) a) and the balanced split (point C21+C22 b). ***Upper gray lines****: When*

operating at the balanced split, the peak of the easier A-BC separation (C11+C12 b) is shifted to the vapor demand of the more difficult AB-C separation (C13+C14 a).

2.2.3 Operational flexibility for the prefractionator

In reality, it is likely that we do not operate exactly at minimum energy, but instead operate either with overpurified products by providing more vapor than needed, or operate with impurities in the product streams by providing less energy (vapor) than needed for sharp separation. Both cases result in a widening of the optimality region into the so-called *flexibility region* of the prefractionator (Figure 4).

If the prefractionator is operated above the optimality region, the energy demand for the separation increases, as investigated in depth by Halvorsen and Skogestad [7]. Looking at it the other way around, if products are overpurified anyway in order to guarantee to match product specifications, this additional vapor also brings more flexibility to the prefractionator operation as the optimality region expands. This can be observed in Figure 4a. Providing $\dot{V}_{C14} > \max\left(\dot{V}_{\min}^{A-BC}, \dot{V}_{\min}^{AB-C}\right)$ means that both peaks in the $\dot{V}_{\min}$ diagram are shifted up, thus both separations are overpurified and not just the easier one. Consequently, the optimality region then widens to a flexibility region and C21+C22 can be operated anywhere between the points a, c, d and e (Figure 4a). This gives room for non-optimality in basically all subcolumns. The profile, that results for an operation within the flexibility region is discussed in more detail in Section 4.4.1 (results).

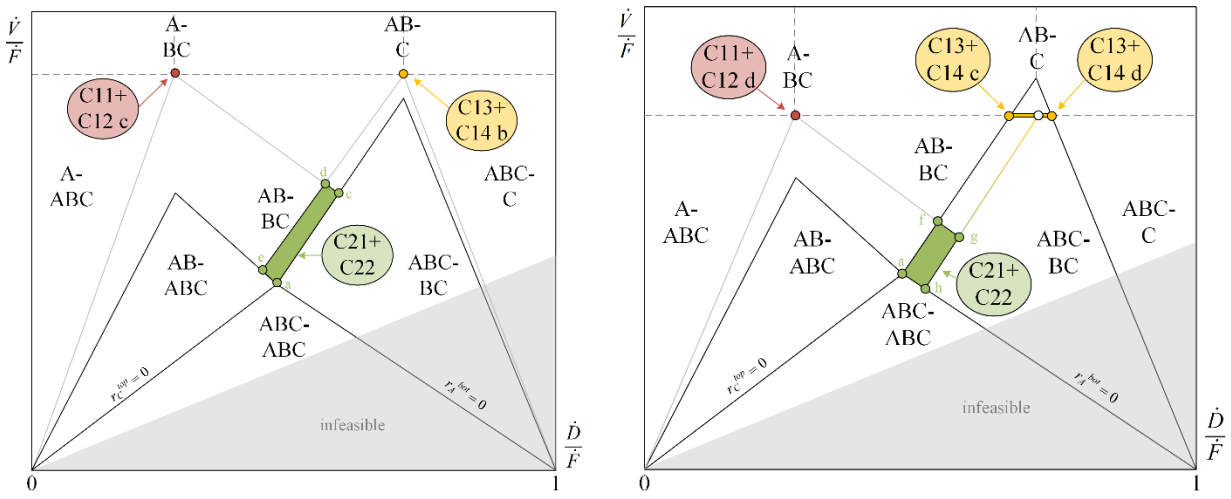

(a) (b)

Figure 4: "Flexibility region" (green box) of a dividing-wall column obtained when either (a) providing $\dot{V}_{C14} > \max\left(\dot{V}_{\min}^{A-BC}, \dot{V}_{\min}^{AB-C}\right)$ to guarantee complete product separation, or (b) allowing impurities in the product streams and providing $\dot{V}_{C14} < \max\left(\dot{V}_{\min}^{A-BC}, \dot{V}_{\min}^{AB-C}\right)$.

On the other hand, it is also likely that impurities are allowed in the product streams, which reduces the required energy demand to be below $\dot{V}_{\min}$ as illustrated in Figure 4b. This reduces the overpurification of the easier separation, which is the separation performed in sections C11+C12 in this example. Consequently, the original optimality region gets smaller (between point a and f). However, additional flexibility can result from the specification of the operating point of the lower main column. The lower border is indicated by C13+C14 c. Here, the side product will contain only component B but part of the middle boiling component is also lost in the bottom product. The upper border is located at point C13+C14 d, where the side draw contains component B and C while the bottom product only contains component C. If the lower main column is operated between the two extrema, there will be component C in the side draw and component B in the bottom product. The flexibility region of the prefractionator between the points C21+C22 a, f, g and h results from the chosen specification of the lower main column, as indicated by the white circle located between C13+C14 c and d. Thus, the lowest flexibility for the prefractionator results from C13+C14 c and the biggest for C13+C14 d. Here, it is important to understand that the operation of the main column can be changed in terms of adapting the product flows to get one pure product. However, then part of the corresponding component is withdrawn in the one of the other product streams.

Of course, it is also possible that both kinds of flexibility regions are combined, if impurities are allowed and additionally more vapor than the minimum one is provided. The resulting shape of the flexibility region can be derived from the $\dot{V}_{\min}$ diagram in a similar manner as presented here.

If the prefractionator is operated outside the flexibility region resulting from the required product specifications and provided energy input, the specifications can no more be fulfilled. However, depending on where the prefractionator is actually operated, this can either be compensated with additional energy input in the main column or the separation task might also become infeasible. In this work, all possible scenarios for a non-optimal operation of the prefractionator are evaluated. For this purpose, the scenario from Figure 4a is chosen as base case. The generalization of the obtained results is discussed in Section 5.

2.3 Pinch zones

To understand the resulting temperature and composition profiles, the concept of pinch zones is crucial [24–26]. Pinch zones are regions inside distillation columns where the composition and thus temperature do almost not change. This happens if many stages are required to achieve very small changes in composition, which is the case at minimum energy consumption. We refer to our recent publication [27,28] about how to understand temperature profiles from pinch zones in conventional two-product distillation columns. Pinches do not actually occur at lower numbers of

theoretical stages, but the temperature and composition profiles still strive in their direction. Thus, they are still visible as slope changes in the temperature profiles. In our publication, seven rules are derived. These are summarized in Table *1* and their use is further explained in Figure 5. Rule 3 mentions "minimum energy lines" which refers to the lines in the $\dot{V}_{\min}$ diagram (Section 2.2). Rule 7 mentions a "clearly" and "poorly" visible pinch. "Poorly visible" refers to pinches are not actually present at a lower number of stages, but where the profiles still strive towards their direction. Thus, they are still visible as slope changes in the temperature profiles.

Table 1*: Rules for reading temperature profiles (derived for a conventional two-product distillation column). *Rules 5 and 6 are revised [28] compared to the original version [27].*

Rule 1	A constant temperature zone (pinch zone) at a column end (top or bottom) indicates an almost pure component in the corresponding product. This pinch zone is observable independently of the total number of stages.
Rule 2	The top and bottom sections can each have a maximum of two pinch zones at the same time. The appearance of two pinches in the same section means that the section is operated at minimum energy. If only one pinch is visible in a section, the product is either over- or underpurified.
Rule 3	At the boundaries between neighboring operating regions, i.e. along the minimum energy lines, the location of pinch zones are the same as in the adjacent regions.
Rule 4	There is an "invariant" pinch temperature when operating at minimum energy or less, which does not change when varying the operating point within the given region of the diagram. The invariant pinch can be observed in the upper part (e.g., if all components are in the bottom product) or the lower part of the column. If all components are present in both product flows, the invariant pinch is above and below the feed stage and has the feed boiling temperature.
Rule 5*	A pinch only on one side of the feed stage means, that all components are present in the product stream at the corresponding column end. In this case, the pinch temperature does not equal the feed boiling point. If this pinch appears in combination with another pinch (rule 2, 3), one component is at the limit to appear but is not actually present (minimum energy case).
Rule 6*	A pinch in the middle of a section indicates that at least two but not all feed components are present in the corresponding product. If this pinch appears in combination with another pinch (rule 2, 3), one component is at the limit to appear but is not actually present (minimum energy case).
Rule 7	A clearly visible pinch in one section in combination with a poorly visible one in the other section is an indication for a nonoptimal feed stage.

The most important facts for understanding pinches in dividing-wall columns are the following:

- A column section has two pinch zones when operated optimally at minimum energy (Rule 2).
- If a pinch appears at one side of the feed stage, all feed components are present in the corresponding product streams (Rule 5).
- Additional pinch zones appear if one or more components disappear totally from a product stream (Rule 6).
- A pinch appears right at the column end if the product is a pure single component (Rule 1), and it appears in the middle of a section if the product contains additional but not all feed components.

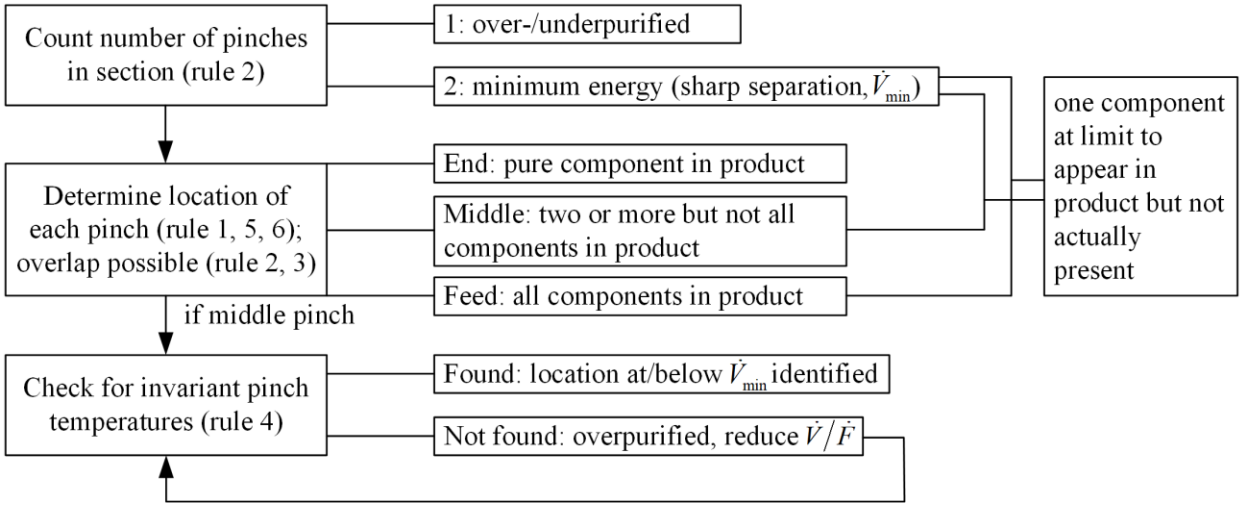

Figure 5: Flowchart for the application of the temperature profile rules in Table 1.

3 Simulation case study

An extensive simulation study was performed to identify and classify non-optimal operation scenarios of the prefractionator of dividing wall columns. The feed mixture is the rather ideal BTX-system (Benzene, Toluene, *p*-Xylene), with liquid activity coefficients modelled with NRTL. More details about the thermodynamic modelling and used parameter sets can be found in the dissertation of Ränger [29] in Section A.2.2 The boiling points T_b of the pure components are 80.1 °C, 110.6 °C and 138.4 °C, respectively. The feed of $\dot{F} = 3\,\mathrm{kmol \cdot h^{-1}}$ is equimolar ($z_A = z_B = z_C = 1/3$) and saturated liquid at 102.2 °C (1 bar). The relative volatilities of the feed mixture are $\alpha_i = [5.60, 2.34, 1]$ (determined in Aspen properties). Based on this, the $\dot{V}_{min}$ diagram of the mixture can be calculated (shortcut approach assuming constant relative volatilities and constant molar flows), see Figures 2 to 4. The highest peak in the diagram is the total energy demand in the dividing wall column, which is $\dot{V}_{min}^{AB-C} = 3.534\,\mathrm{kmol \cdot h^{-1}}$. From the $\dot{V}_{min}$ diagram also

the optimality and flexibility region can be read as described in Sections 2.2.2 (Figure 3) and 2.2.3 (Figure 4).

Detailed simulations of the temperature profiles are performed using Aspen Plus V11. The dividing wall column is represented by three thermally coupled RadFrac columns with 60 stages each, so 180 stages in total. Because the separation is relatively simple, with large differences in component boiling points, 60 stages is enough to give almost pure products if operated properly. The feed in each subcolumn is in the middle (stage 30).

For all simulations, the product flows are set based on Equation (3) with $\dot{F} = 3\,\mathrm{kmol}\cdot\mathrm{h}^{-1}$ resulting in $\dot{D}_{C11} = \dot{S} = \dot{B}_{C14} = 1\,\mathrm{kmol}\cdot\mathrm{h}^{-1}$. The provided vapor flow at the main column bottom $\dot{V}_{C14}$ is either set at the minimum energy demand $\dot{V}_{\min}^{AB-C}$ or 8 % higher at $1.08\cdot\dot{V}_{\min}^{AB-C}$ (in the following denoted as excess energy). This minimum energy demand corresponds to the prefractionator operation within the optimality region (see Section 2.2.2). Then, the liquid and vapor flows fed to the prefractionator top and bottom are varied outside their optimal range, which is equivalent to a change in the liquid and vapor split ratios, R_L and R_V. The detailed simulation inputs are summarized in Table 2, which should be read in combination with Figure 10.

All simulations are evaluated by considering the composition and temperature profiles. To make the results more general, the plots use the relative temperature t defined as

$$t = \frac{T - T_{b,Benzene}}{T_{b,p-Xylene} - T_{b,Benzene}} \tag{15}.$$

The relative temperature is in the range $t = 0$ (boiling point of light component, Benzene) to $t = 1$ (boiling point of heavy component, *p*-Xylene). The relative boiling point of the middle component (Toluene) is $t_{b,Toluene} = 0.52$ for this mixture. The relative boiling point of the equimolar feed mixture is $t_{b,Feed} = 0.38$.

In addition to the temperature profiles, the net components flow w inside the column are visualized by the colored flows in part b of Figure 12 to Figure 20. The net component flow is defined in equation (16), where the index n denotes a stage and n+1 the one below, y is the molar fraction in the vapor phase and x in the liquid phase.

$$w_i = y_{i,n+1}\cdot\dot{V}_{n+1} - x_{i,n}\cdot\dot{L}_n \tag{16}$$

The net component flow indicates the overall path of a component inside the column. If it is positive the flow is in the direction of the column top and if it is negative to the column bottom.

4 Results

In this section, first the "perfect" operation of a dividing wall column with a side condenser/evaporator (Figure 2b) is evaluated (Section 4.1). Next, a typical three-product dividing wall column is studied. It is without a side condenser (Figure 3b) and with the main column operated at minimum energy, $\dot{V}_{C14} = \max\left(\dot{V}_{\min}^{A-BC}, \dot{V}_{\min}^{AB-C}\right)$. Results in terms of temperature and composition profiles are shown for the prefractionator operated at both the preferred split (Section 4.2.1) and the balanced split (Section 4.2.2). Section 4.3 evaluates the feasible operating range of the prefractionator in the case of non-optimal operation. Here, feasible refers to the physically feasible range of vapor and liquid flows that can be fed to the prefractionator, determined based on internal mass balances. Next, in Section 4.4, it is assumed that the main column is operated with 8 % additional energy, $\dot{V}_{C14} = 1.08 \cdot \max\left(\dot{V}_{\min}^{A-BC}, \dot{V}_{\min}^{AB-C}\right)$, so that the optimality region widens into a flexibility region. All feasible non-optimal operating cases of the prefractionator are summarized and corresponding profiles and net component flows are evaluated. Finally, Section 4.5 focuses on how to detect non-optimal prefractionator operation based on its temperature profile.

4.1 Profiles at "perfect" operation with side condenser/reboiler (prefractionator at $\dot{V}_{C21} = \dot{V}_{\min}^{AB-BC}$, main column at $\dot{V}_{C11} = \dot{V}_{\min}^{A-BC}, \dot{V}_{C14} = \dot{V}_{\min}^{AB-C}$)

As described in Section 2.2.1, perfect operation without remixing can be observed if all three subcolumns operate at their minimum energy demand, which is usually only possible with a side evaporator (if the AB-C peak is lower) or side condenser (if the A-BC peak is lower as in this case study; Figure 2). Figure 6 shows the resulting composition and temperature profile for the BTX separation with a side condenser.

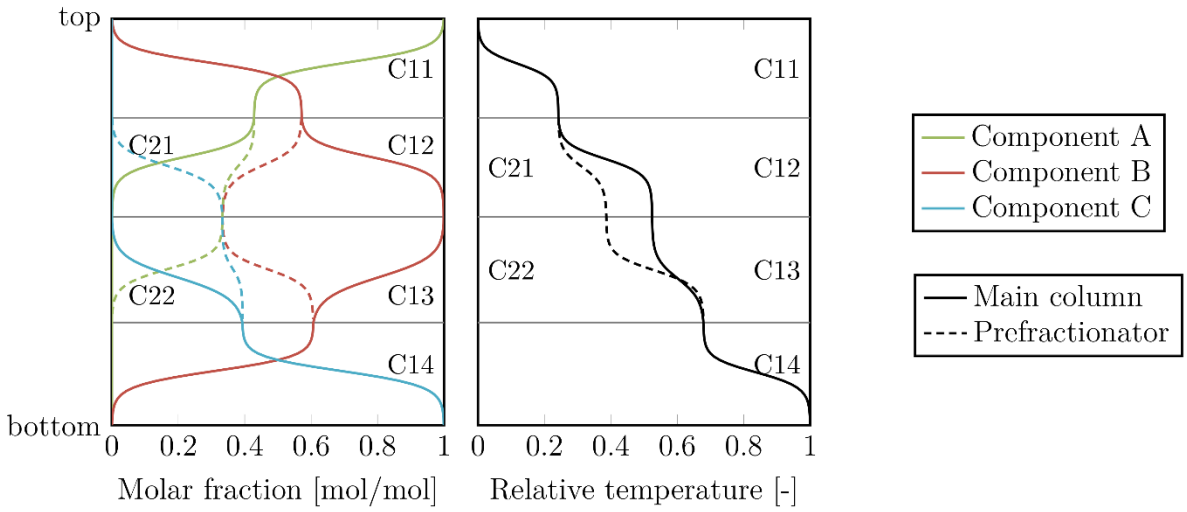

Figure 6: (a) Liquid composition and (b) temperature profiles for "perfect" dividing wall column operation with side condenser (Figure 2b). The prefractionator operates at the preferred split (minimum energy for AB-BC separation) and the side condenser ensures minim energy $\left(\dot{V} = \dot{V}_{\min}\right)$ *for both separations in the main column (A-BC and AB-C), resulting in no remixing zones. See Table 2 for specifications.*

The composition profile of the prefractionator in Figure 6a (dashed lines) shows that the mole fraction of component C (blue) reaches zero shortly before the top (C21) and increases smoothly towards the bottom (C22). The same applies in the opposite way for component A (green). Component B (red) distributes to the top and the bottom product and the mole fraction reaches a minimum at the feed stage. The compositions at the two ends of the prefractionator (dashed lines) equals the pinch compositions at the feed stage in the main column (solid lines), therefore the profiles here merge smoothly. Within the main column, the fraction of component A (green line) increases steadily towards the top (C11), while the fraction of component C (blue line) increases towards the bottom (C12). Considering the upper and lower main column together, there is a maximum fraction of component B (red line) at the side draw (between C12 and C13). Figure 6b shows the corresponding smooth temperature profiles.

All three subcolumns have two pinches in each section, thus there are 12 pinches in total. This indicates minimum energy operation in all sections (Rule 2 from Table *1*). In all subcolumns (each consisting of two sections), there are pinches above and below the feed stage and at the column ends. The pinch above and below the feed stage in combination with a second pinch means that all feed components are about to appear in the corresponding product streams, however one component is right at the border to appear and thus is not actually present (Rule 5 in Table *1*. Thus, they are still visible as slope changes in the temperature profiles.

Table *1*). In the prefractionator, this means that component C reaches a mole fraction of zero close to the prefractionator top and component A reaches zero close to the prefractionator bottom. Thus,

the two main column parts both have a binary feed stream. The other pinches in the main column are located at the subcolumn top and bottom ends, which means that pure products are obtained (Rule 1 in Table *1*). Interestingly, this is also the case for the prefractionator. If the same separation would be performed in a conventional distillation column, the two pinches at the ends of the prefractionator would instead appear in the middle of the two sections (Figure 9b in [27], Rule 6 from Table *1*).

The reason they appear at the ends of the prefractionator is that the feed pinch compositions in the main columns are the same as the pinch compositions at the end of sections C21 and C22. Thus, compared to a conventional distillation column with evaporator/condenser, remixing zones at the column ends are avoided in the prefractionator of a dividing wall column. This makes the dividing wall (Petlyuk) column "more optimal" (with less exergy loss) than a structure with a "normal" prefractionator (with a condenser and reboiler, rather than taking reflux and vapor from the main column) performing the same separation task.

However, it is not common to operate a dividing wall column with a side condenser/evaporator. The following Sections evaluate how the profiles change if the dividing wall column is operated at the higher of the two peaks in the $\dot{V}_{\min}$ diagram, meaning that either the easier separation in the main column can be overpurified or the prefractionator can be overpurified.

4.2 Profiles at boundaries of optimality region (main column at $\dot{V}_{C14} = \dot{V}_{C11} = \dot{V}_{\min}^{AB-C}$)

Subsection 4.2.1 shows profiles with the prefractionator operated at the preferred split and Subsection 4.2.2 with the prefractionator operated at the balanced split.

4.2.1 Prefractionator at preferred split $\left(\dot{V}_{C21} = \dot{V}_{\min}^{AB-BC}\right)$

Figure 7 shows the composition and temperature profiles with the prefractionator operated at minimum energy (at the preferred split) (Figure 3 with prefractionator at point a), the lower main column at minimum energy and the upper main column with excess energy and thus overpurified.

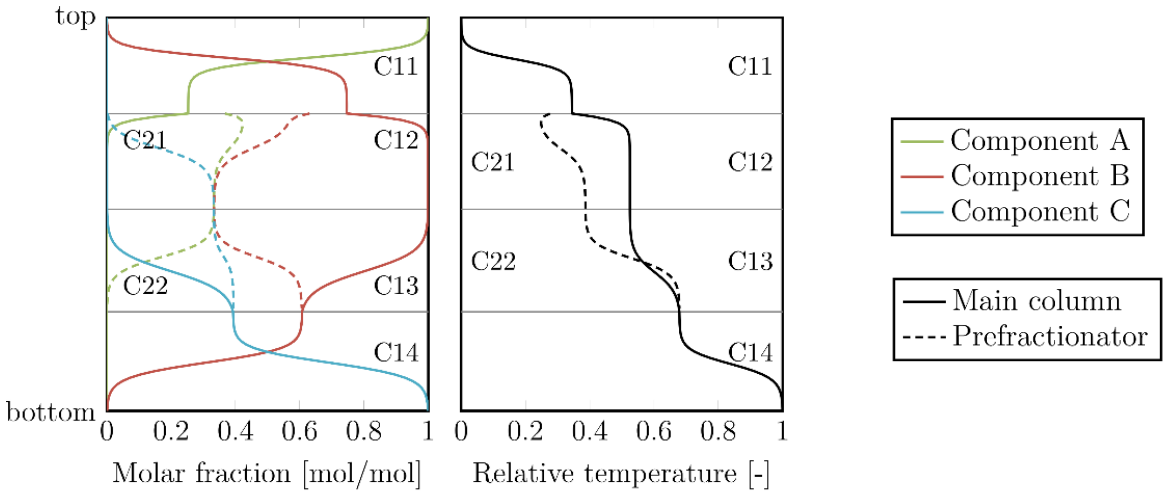

Figure 7: (a) Liquid composition and (b) temperature profile of dividing wall column with the prefractionator operated at the preferred split (minimum energy) and the main column operated at $\dot{V}_{C14} = \dot{V}_{\min}^{AB-C} \approx \dot{V}_{C11}$ *(overpurification in top). See Table 2 for specifications.*

The profiles of the lower main column (C13 and C14) and lower prefractionator section (C22) are similar like to "perfect" operation (Figure 6), although there are differences in the upper sections. Due to the overpurification, component A (solid green line) is no more at the limit to appear in the side draw, so the pinch disappears in the top part of section C12 (below the upper feed in the main column). The temperature of the pinch at the other side of the feed (lower end of C11) increases and no longer equals the pinch composition in the upper prefractionator. This shifts the pinch in the upper prefractionator towards the middle of section C21. Based on the results in Section 4.1, this is an indication of remixing and thus exergy losses. However, this remixing is not a problem in this case, as excess energy is provided for the easier separation.

4.2.2 Prefractionator at balanced split

Figure 8 shows the profiles with the prefractionator operated at the balanced split (with excess energy and thus overpurified in the bottom) (Figure 3 with prefractionator at point b) and the upper and lower main column operated at minimum energy.

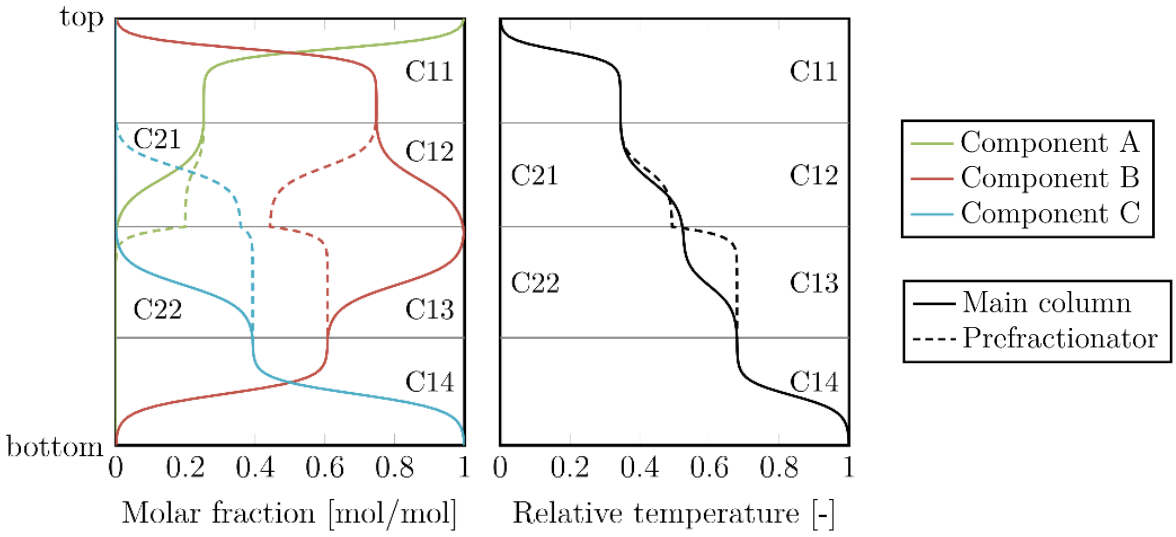

448 *Figure 8: (a) Liquid composition and (b) temperature profile of dividing wall column with the*
449 *prefractionator operated at the balanced split (excess energy, resulting in overpurification of A in the*
450 *bottom of the prefractionator) and the main column operated at* $\dot{V}_{C14} = \dot{V}_{\min}^{AB-C} \approx \dot{V}_{C11}$ *(minimum energy).*
451 *See Table 2 for specifications.*

452 At the balanced split, the lower section C22 of the prefractionator operates with excess energy
453 resulting in overpurification of component A in the bottom and the disappearance of the pinch at
454 the top of section C22 (dashed lines) .Component C is still at the limit to be distributing (line
455 $r_C^{top} = 0$ in Figure 3) but not A (it is no longer on line $r_A^{bot} = 0$). The upper part of the main column
456 is operated at minimum energy, thus there a pinch on both sides of the upper feed stage (C11 and
457 C12). Correspondingly, there is a pinch at the prefractionator top (C21) at the same location as the
458 pinch in the main column; similar to the ideal case in Figure 6.

459 ## 4.3 Feasible operating range of prefractionator

460 In order to find out which non-optimal operating points are possible in the prefractionator, this
461 section analyzes the entire possible range of liquid and vapor split ratios, R_V (Equation (11) and R_L
462 (Equation (12)). As stated before, the term feasible means that mass balances allow this
463 prefractionator operation with all flowrates being non-negative. For a real plant without vapor split
464 manipulation but a careful hydraulic design some of the regions may seem unrealistic. But if, for
465 example, one column part is flooded or blocked, some of these boundary cases may still occur, so
466 the whole reachable range will be evaluated. To map the feasible vapor and liquid split ratios into
467 the $\dot{V}_{\min}$ diagram of the prefractionator, an expression for $\dot{V} = \dot{V}_{C21} = f\left(\dot{D}_{C21}\right)$ is required.

468 For the vapor split ratio, rearranging Equation (11) and inserting Equation (8) results in

469 $$\frac{\dot{V}_{C21}}{\dot{F}} = R_V \cdot \frac{\dot{V}_{C14}}{\dot{F}} + \frac{\dot{V}_F}{\dot{F}} = R_V \cdot \frac{\dot{V}_{C14}}{\dot{F}} + (1-q) \qquad (17).$$

From this it follows that at a given energy input at the column bottom (constant $\dot{V}_{C14}$), different vapor split ratios R_V result in parallel horizontal lines in the $\dot{V}_{\min}$ diagram (green lines) in Figure 9. With a liquid side draw, the feasible range of the vapor split ratio is between $0 \le R_V \le 1$, which results in the following extreme cases for the vapor flow in the top of the prefractionator:

$$R_{V,\min} = 0: \ \frac{\dot{V}_{C21}}{\dot{F}} = (1-q) \tag{18}$$

$$R_{V,\max} = 1: \ \frac{\dot{V}_{C21}}{\dot{F}} = \frac{\dot{V}_{C14}}{\dot{F}} + (1-q) \tag{19}$$

Similarly, in terms of the liquid split ratio, Equation (20) results (orange lines in Figure 9)

$$\frac{\dot{V}_{C21}}{\dot{F}} = R_L \cdot \left(\frac{\dot{V}_{C14}}{\dot{F}} + \frac{\dot{V}_F}{\dot{F}} - \frac{\dot{D}_{C11}}{\dot{F}} \right) + \frac{\dot{D}_{C21}}{\dot{F}} = R_L \cdot \left(\frac{\dot{V}_{C14}}{\dot{F}} + (1-q) - \frac{\dot{D}_{C11}}{\dot{F}} \right) + \frac{\dot{D}_{C21}}{\dot{F}} \tag{20}$$

Here $\dot{D}_{C21}/\dot{F}$, is the net flow that leaves the top of the prefractionator (at non-optimal operation, it may be negative or greater than 1). From Equation (20), different liquid split ratios R_L result in parallel straight lines with slope +1 as a function of $\dot{D}_{C21}/\dot{F}$, as indicated by orange lines in Figure 9. The lower limit of the liquid split ratio is $R_L = 0$ (no liquid is provided to the prefractionator), and the relationship becomes

$$R_{L,\min} = 0: \ \frac{\dot{V}_{C21}}{\dot{F}} = \frac{\dot{D}_{C21}}{\dot{F}} \tag{21}$$

If the side stream $\dot{S}$ is in liquid state, as assumed in this work, there has to be enough liquid in section C12. This results in the following upper limit on R_L:

$$R_{L,\max} = \frac{\dot{L}_{C11} - \dot{S}}{\dot{L}_{C11}} = \frac{\dot{V}_{C11} - \dot{D}_{C11} - \dot{S}}{\dot{V}_{C11} - \dot{D}_{C11}} = \frac{\dot{V}_{C14} + \dot{V}_F - \dot{D}_{C11} - \dot{S}}{\dot{V}_{C14} + \dot{V}_F - \dot{D}_{C11}} \tag{22}$$

which is less than 1. Note that in the ideal case with pure products the distillate product flow $\dot{D}_{C11}$ equals the mole flow of component A in the feed and the mole flow of the side draw $\dot{S}$ equals the flow of component B in the feed stream. With this and Equation (8), Equation (22) becomes

$$\text{Ideal case: } R_{L,\max} = \frac{\dot{V}_{C14} + (1-q-z_A-z_B)\cdot\dot{F}}{\dot{V}_{C14} + (1-q-z_A)\cdot\dot{F}} \tag{23}$$

For the more general case in Equation (22) the following mapping results for the maximum liquid split in the $\dot{V}_{\min}$ diagram:

$$R_{L,\max}: \ \frac{\dot{V}_{C21}}{\dot{F}} = \frac{\dot{V}_{C14}}{\dot{F}} + (1-q) - \frac{\dot{D}_{C11}}{\dot{F}} - \frac{\dot{S}}{\dot{F}} \tag{24}$$

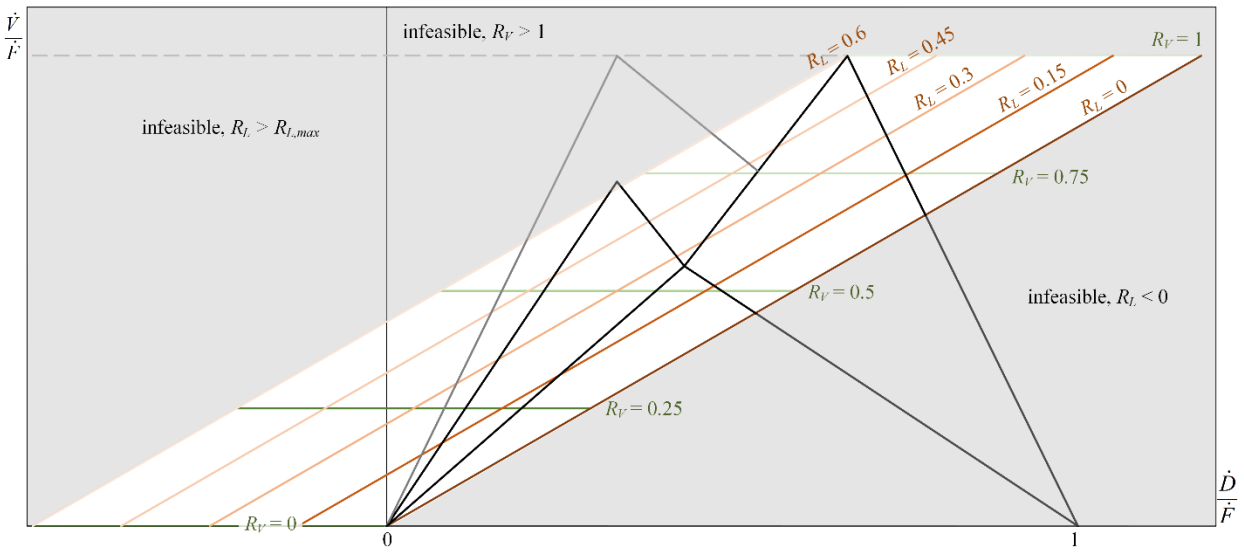

Figure 9: $\dot{V}_{\min}$ diagram for operation of the prefractionator (C21+C22) for a liquid feed (q = 1) with lines of constant vapor split (green lines) and constant liquid split (orange lines). The white area shows the feasible region of operation. $\dot{D} = \dot{D}_{C21}$ (x-axis) is the net distillate flow from the prefractionator (Equation (5))*, which may be negative or above 1. $\dot{V} = \dot{V}_{C21}$ (y-axis) is the vapor flow in the top of the prefractionator. The product flows are based on Equation* (3).

Based on these considerations and the assumption that for our case study the feed is a saturated liquid $\left(\dot{V}_F = 0,\ q = 1\right)$ the feasible operating range of the prefractionator can be visualized as shown by the white area in Figure 9. Gray areas indicate infeasible regions. As already noted, the prefractionator can also be operated with $\dot{D}_{C21}/\dot{F}$ negative or above 1 (also mentioned in [18] on page 104). This is a major difference compared to a conventional distillation column which has to fulfil Equation (6), resulting in $\dot{D}/\dot{F}$ being between 0 and 1. The broader range for the prefractionator arises from the fact, that only $\dot{V}_{C22}$ and $\dot{L}_{C21}$ have to be positive (Equation (7)). Then, in Equation (5) it may happen that the liquid flow is larger than the vapor flow, resulting in and a negative value for the net distillate flow $\dot{D}_{C21}$.

Note that the lines of constant split ratios (orange and green lines in Figure 9) shift uniformly with changes in the amount of $\dot{V}_{C14}/\dot{F}$ provided at the main column bottom. Consequently, changing the vapor input while maintaining the same split ratios causes a shift of the resulting operating point of the prefractionator. It may happen that the new operating point is outside the flexibility region. All non-optimal operating scenarios are discussed in more detail in the following Section 4.4.

4.4 Classification of feasible prefractionator operation cases with excess energy in the main column $\dot{V}_{C14} = 1.08 \cdot \dot{V}_{\min}^{AB-C} \approx \dot{V}_{C11}$

Based on extensive simulations described in Section 3, the prefractionator operation cases are summarized by the labeled regions in Figure 10. Note that in all cases, the main column operation is fixed by setting the product flows as in Equation (3) and providing 8 % excess vapor at the main column bottom. Excess vapor means that more vapor is provided than required in the main column with the prefractionator operated in the optimality region (see Sections 2.2.2 and 2.2.3). In other words, if the liquid and vapor split ratios are optimal, the energy provided in the main column is more than sufficient to perform a complete separation Then, the liquid and vapor split ratios R_L and R_V are varied towards non-optimal values to change the prefractionator operation. The specifications used for all simulations of the BTX case study are summarized in Table 2.

It was found that composition and temperature profiles look similar when the prefractionator is operated within one region (but at different points) of the original $\dot{V}_{\min}$ diagram. However, it was also found that the liquid and vapor recycle from the main column introduces additional regions $\dot{V}_{\min}$ diagram. Hence, the $\dot{V}_{\min}$ diagram was extended in Figure 10 to cover all feasible cases. In Figure 10, the endings .1 and .2 indicate "symmetrical" cases, that either apply for component A or C, and the endings .a and .b indicate cases with same products from the prefractionator but with differences in the main columns.

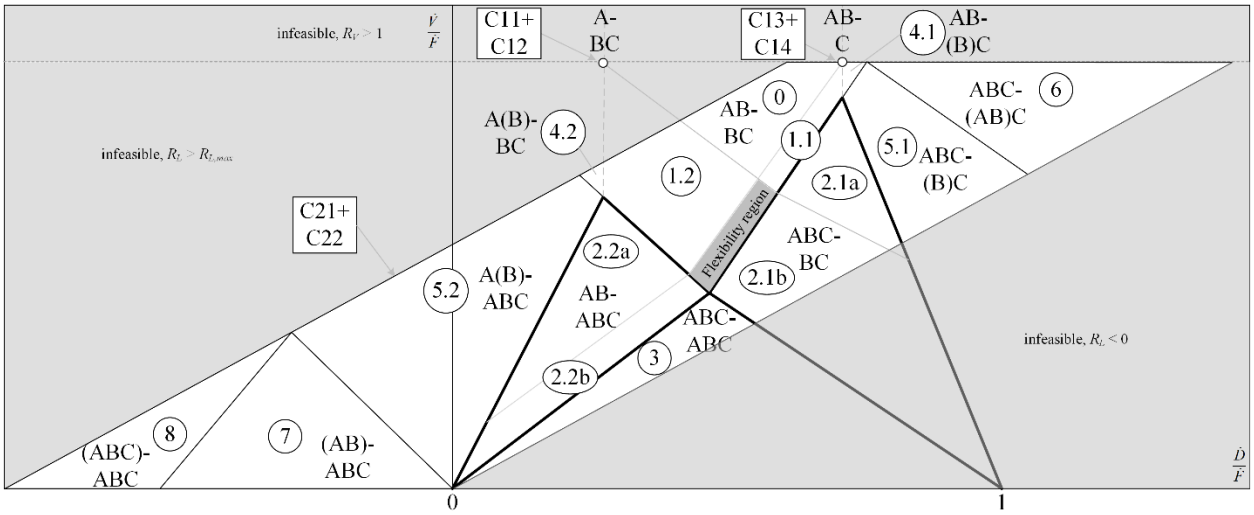

Figure 10: Feasible non-optimal operation regions of the prefractionator (C21+C22) with excess energy in the main column (related to optimal prefractionator operation), $\dot{V}_{C14} = \dot{V}_{C11} = 1.08 \cdot \dot{V}_{\min}^{AB-C}$, found for the BTX case study. Bold lines represent the original $\dot{V}_{\min}$ diagram. Components obtained in the top product of the prefractionator are given before the hyphen and components in the bottom product behind the hyphen. Components in brackets are circulating around the dividing wall.

In the following, the composition and temperature profiles and net component flows for all cases are shown. First, Section 4.4.1 shows the profiles for an operation within the flexibility region. Section 4.4.2 focuses on cases 0 and 1 (1.1 and 1.2), which represent overpurification of the prefractionator. As a consequence, since the main column provides reflux and boilup to the prefractionator, the energy demand of either the upper, lower or both parts of the main column increases. Section 4.4.3 summarizes cases 2 and 3, which represent an underpurification of the prefractionator as it is operated below the $\dot{V}_{\min}$ border (although the reboiler in the main column is supplied with 8 % excess vapor compared to the case when R_L and R_V were set optimally). Then, two or three components distribute within the prefractionator instead of only the middle-boiling component (B) which means that there is at least one ternary feed to the main column. Section 4.4.4 focuses on the cases 4, 5, 6, 7 and 8 with the commonality that there is at least one component circulating around the dividing wall. Circulating components are indicated by parenthesis in Figure 10. At low or negative $\dot{D}/\dot{F}$ ratios, the circulation is counterclockwise, while it is clockwise at high $\dot{D}/\dot{F}$ ratios. Note that most of these cases are delimited by borders in the $\dot{V}_{\min}$ diagram.

Table 2: Specifications used for BTX case study. ≛ Vapor fraction side condenser = 0.315, resulting in $\dot{V}_{C11} = 2.565\ \mathrm{kmol \cdot h^{-1}}$ *at top main column. In all other cases,* $\dot{V}_{C11} \approx \dot{V}_{C14}$.

Case (see Figure 2, 3 and 10)	Figure	$\dot{V}_{C14}\left[\mathrm{kmol \cdot h^{-1}}\right]$ Vapor bottom main column	$\dot{V}_{C22}\left[\mathrm{kmol \cdot h^{-1}}\right]$ Vapor to bottom prefractionator	$\dot{L}_{C21}\left[\mathrm{kmol \cdot h^{-1}}\right]$ Liquid to top prefractionator
Perfect (with side condenser)	Figure 6	3.565*	1.9680	0.7170
Preferred	Figure 7	3.565	1.9670	0.7064
Balanced	Figure 8	3.565	2.8570	1.2590
Flexibility	Figure 11	3.863 = 1.08 · 3.565	2.3180	0.9450
0	Figure 12	3.863	3.3611	1.7466
1.1	Figure 13	3.863	3.2840	1.5800
2.1a	Figure 14	3.863	3.1500	1.1700
2.1b	Figure 14	3.863	2.7040	0.7330
3	Figure 15	3.863	1.3140	0.2860
4.1	Figure 16	3.863	3.7000	1.7700

5.1	Figure 17	3.863	3.0910	0.5730
6	Figure 18	3.863	3.5830	0.2860
7	Figure 19	3.863	0.4640	1.3460
8	Figure 20	3.863	0.3860	1.7470

554

555 4.4.1 Operation within the flexibility region

556 Figure 11 shows the composition and temperature profiles for a dividing wall column whose
557 prefractionator is operated in the middle of the flexibility region (see Figure 10).

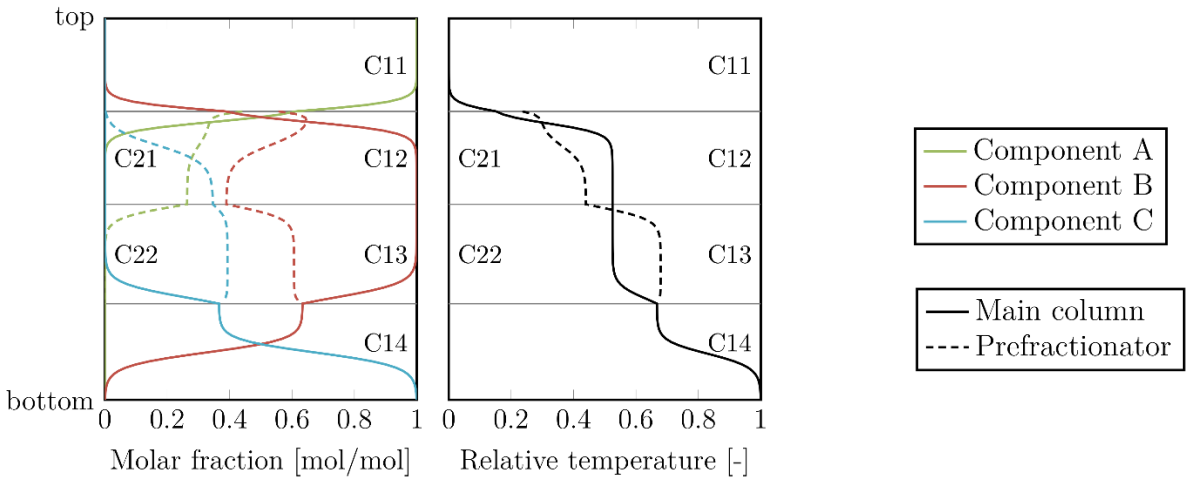

558 *Figure 11: Profiles for prefractionator operation within the flexibility region by providing*
559 $\dot{V}_{C14} = 1.08 \cdot \dot{V}_{\min}^{AB-C}$ *in the main column. See Table 2 for specifications.*

560 The fraction of component C still reaches zero close to the top end of the prefractionator (C21,
561 blue dashed line), but component A disappears before the bottom of the prefractionator (green
562 dashed line), which indicates that the lower part of the prefractionator (C22) is overpurified. This
563 is supported by the fact that only one pinch is visible instead of two in section C22) (Rule 2 in
564 Table *1*). In the upper part of the prefractionator (C21) there are still two pinches visible, thus it is
565 operated close to minimum energy. This imbalance between the upper and lower part of the
566 prefractionator can be seen as rather abrupt temperature and composition changes close to the feed
567 stage.

568 The upper main column has a “long” pinch at the top end (C11) caused by overpurification, but no
569 pinch above the feed from the prefractionator. Both are clear indications of overpurification. The
570 missing pinch results in a misfit between the compositions at the bottom of C11 and the remixing

zone at the top of the prefractionator (C21), shifting the pinch to the middle and causing a maximum in the fraction of component B in the prefractionator.

In the lower main column (C13+C14) there are in total three pinches. The one below the side product is very long, which results from overpurification of component B in the side product. This can also be observed in the composition profile as component B reaches a high purity already at stage 75 while the side draw is at stage 60. The lowest section of the main column (C14) has two pinches, thus is close to minimum energy operation.

The profiles are different at other locations within the flexibility region (not at the boundaries) but the general pattern is similar.

4.4.2 Excess energy to prefractionator: Overpurification of separation in prefractionator and underpurification of main column (cases 0, 1.1, 1.2)

This Section summarizes cases with excess vapor to the prefractionator (increased R_V), resulting in an overpurified prefractionator, either in both ends (C11 and C12, case 0) or in only the lower part (C22, case 1.1) or only the upper part (C21, case 1.2). This is similar to the previous Section 4.4.1 for the lower part. However, in this section a too high value of the vapor split (R_V) implies that too little energy is supplied to the main column resulting in impurities in the product streams. Note that in all these cases still pure product streams could be obtained when increasing the overall energy input in the main column $\dot{V}_{C14}$.

Figure 12 shows the composition profile and net component flows for case 0. From the composition profile of the prefractionator (dashed line) in Figure 12a it can be seen that the fraction of component C reaches zero significantly before the top (C21). The overpurification in section C22, which is also present within the flexibility region, gets more pronounced and the fraction of component A reaches zero shortly below the feed inlet. Providing too much vapor to the prefractionator means providing too little vapor in sections C12 and C13 in the main column. As a result, the pinches at the top of C11 and bottom of C14, indicating pure top and bottom products, disappear and instead two long pinches appear in the middle of the upper and lower main column. This indicates an underpurification which could have been avoided by using more total energy input.

Figure 12b shows the corresponding net flows of the components through the dividing wall column. It is clear that the prefractionator performs the desired separation between components A and C, however both separations in the main column are not sharp.

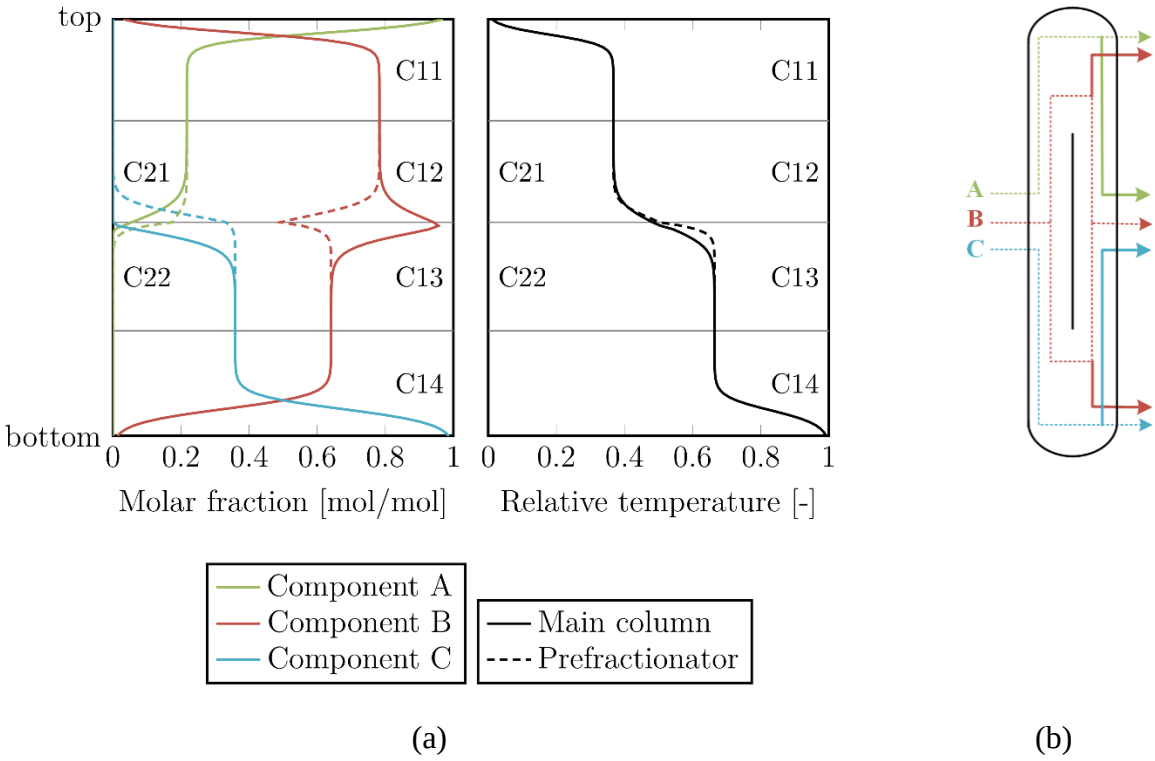

Figure 12: Case 0. (a) Liquid composition and temperature profile and (b) net flow of components inside the column for non-optimal prefractionator operation providing $\dot{V}_{C14} = 1.08 \cdot \dot{V}_{\min}^{AB-C}$ *in the main column. Dotted lines show original optimal path of the components and solid lines represent different paths for non-optimal operation. See Table 2 for specifications.*

Figure 13 shows the profiles and flows for Region 1.1, in which only the lower prefractionator (C22) part is over-purified. The fraction of component C still reaches zero shortly below the feed stage and no further composition change happens in the lower part of the section, while the fraction of component A reaches zero shortly before the top end of C21. Sending excess vapor to the prefractionator increases the energy demand of the upper main column. Again, as not sufficient energy is provided anymore, a pinch appears in the middle of the upper main column. From Figure 13b it can be seen that component B is present in the top product and component A in the side product.

Region 1.2 is not shown here, as the observations are similar as for Region 1.1, except that the vapor flow imbalance appears in the upper prefractionator part C21 and the lower main column.

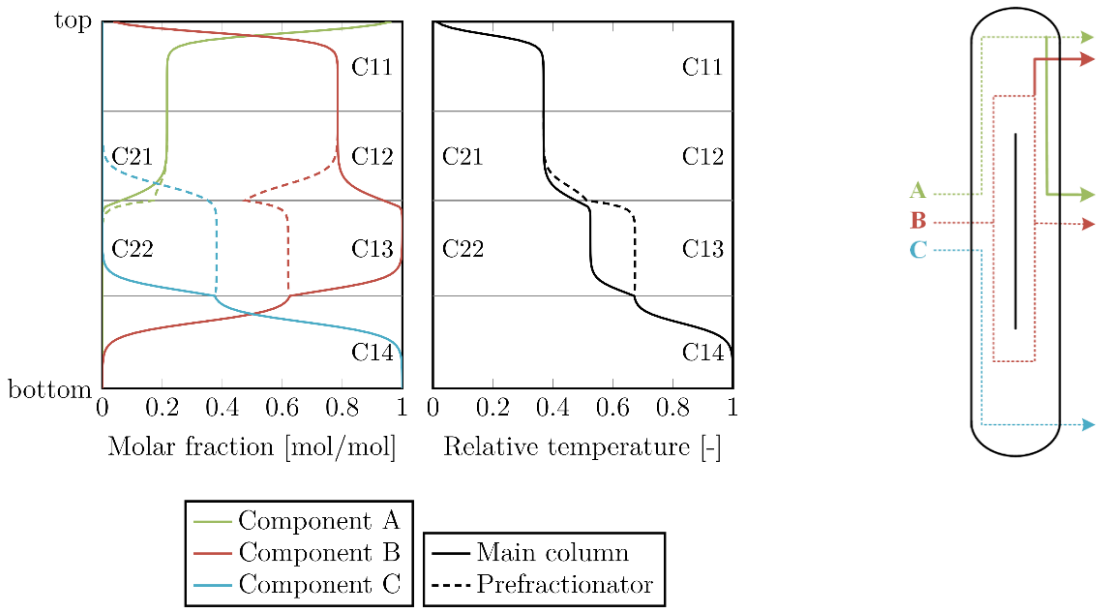

Figure 13: Case 1.1 (a) Liquid composition and temperature profile and (b) net flow of components inside the column for non-optimal prefractionator operation providing $\dot{V}_{C14} = 1.08 \cdot \dot{V}_{\min}^{AB-C}$ *in the main column. Dotted lines show original optimal path of the components and solid lines represent different paths for non-optimal operation. For Region is 1.2 the flow paths in the main column are mirrored to the lower part. See Table 2 for specifications.*

4.4.3 Underpurification in prefractionator (cases 2.1a, 2.1b, 2.2a, 2.2b, 3)

This Section summarizes the cases, in which the prefractionator is underpurified, which means that either the top or bottom product of it or both contain more than two components. Either component C also leaves at the top of the prefractionator (C21, case 2.1), or component A at the bottom (C22, case 2.2). In case 3 all components leave at the top and bottom. In any case, this operation leads to impure products which cannot be avoided with more energy input.

Figure 14 shows the profiles and flows of case 2.1, when component C distributes within the prefractionator and partially leaves at the top (C21). It was found that there are two types of profiles/flow paths can be observed in the main column, which appears depends on the prefractionator operating point within the region ABC-AB of the $\dot{V}_{\min}$ diagram. The location of the border between the two subregions .a and .b can be seen in Figure 10. Note that region .b only exists if $\dot{V}_{C14} > \dot{V}_{\min}^{AB-C}$ is provided in the main column.

Figure 14a shows the composition profile for case 2.1a and Figure 14b the corresponding net flow paths of the components. As component C partly leaves the prefractionator at the top, it can be found in the side product. Additionally, the separation in the upper main column is not complete, resulting in component B in the top and component A in the side product.

637 Figure 14c shows the composition profiles for the operation in case 2.1b and the corresponding
638 net flow paths can be seen in Figure 14d. Different to case 2.1a, the separation in the upper main
639 column is complete and pure component a can be obtained in the top product. The same applies in
640 the opposite way for case 2.2.

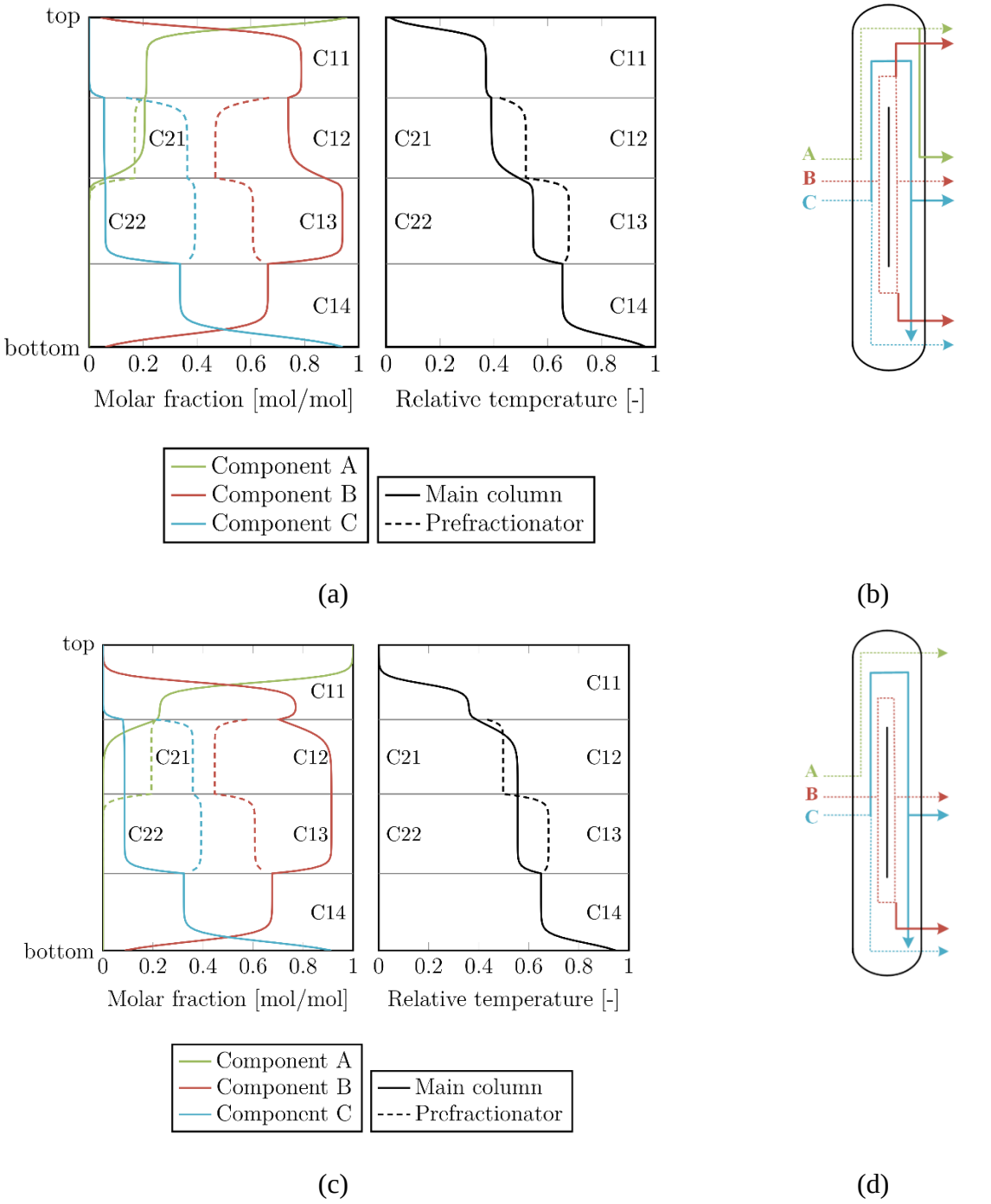

Figure 14: Case 2.1a (a) Liquid composition and temperature profile and (b) net flow of components inside the column for non-optimal prefractionator operation providing $\dot{V}_{C14} = 1.08 \cdot \dot{V}_{\min}^{AB-C}$ *in the main column. For case 2.2 the flow paths of components A and C are switched. (c) and (d) the same for case 2.1b. Dotted lines in (b) and (d) show original optimal path of the components and solid lines represent different paths for non-optimal operation. See Table 2 for specifications.*

Figure 15a gives the composition profile of an operation in case 3 and Figure 15b the corresponding net flow paths. As all components leave the prefractionator at the top and bottom,

all products are impure. There is additionally component B in the top product, components A and C in the side product and component B in the bottom product.

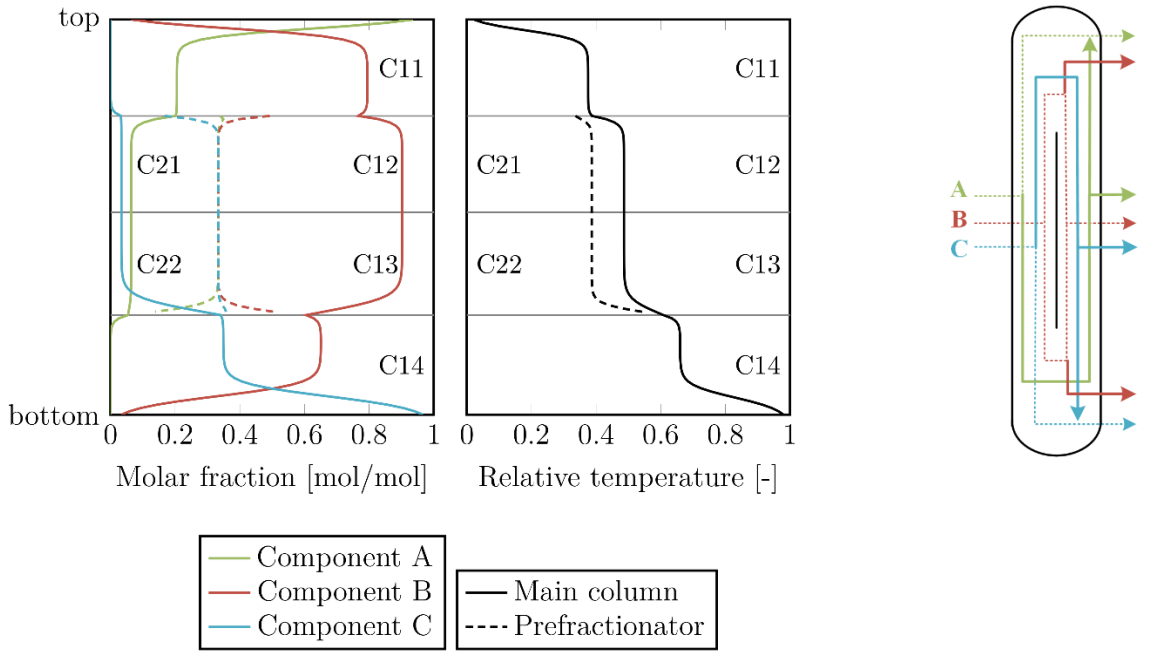

(a) (b)

Figure 15: Case 3 (a) Liquid composition and temperature profile and (b) net flow of components inside the column for non-optimal prefractionator operation providing $\dot{V}_{C14} = 1.08 \cdot \dot{V}_{\min}^{AB-C}$ *in the main column. Dotted lines show original optimal path of the components and solid lines represent different paths for non-optimal operation. See Table 2 for specifications.*

4.4.4 Cases with circulating components (cases 4.1, 4.2, 5.1, 5.2, 6, 7, 8)

This Section summarizes cases with circulation of at least one component.

On the right side of the $\dot{V}_{\min}$ diagram in Figure 10, thus at high $\dot{D}/\dot{F}$ ratios, the circulation is clockwise with reverse flow below the dividing wall. In case 4.1 (Figure 16) component B circulates and distributes in the upper main column between the top and side product. Due to mass balances, component A is present in the side draw. With higher $\dot{D}/\dot{F}$ ratios in case 5.1 (Figure 17) component C starts to distribute within the prefractionator, and leaves it partially at the top. As a consequence, it ends up as additional impurity in the side draw. Again, due to mass balances, component B is also present in the bottom product. With a further increase of $\dot{D}/\dot{F}$ towards case 6 (Figure 18), additionally component A starts to circulate below the dividing wall.

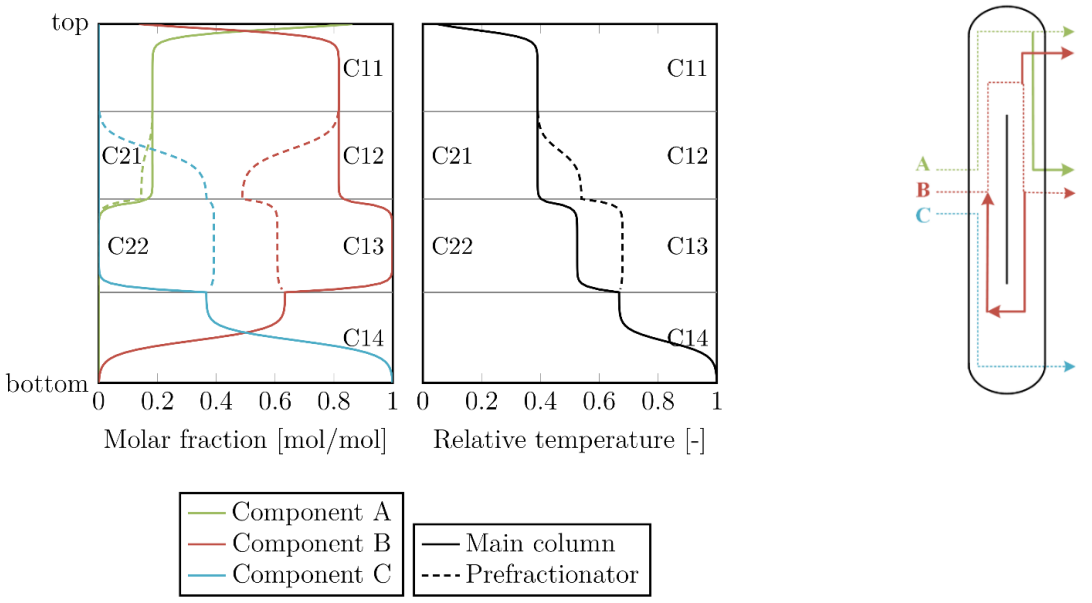

Figure 16: Case 4.1 (a) Liquid composition and temperature profile and (b) net flow of components inside the column for non-optimal prefractionator operation providing $\dot{V}_{C14} = 1.08 \cdot \dot{V}_{\min}^{AB-C}$ *in the main column. Dotted lines show original optimal path of the components and solid lines represent different paths for non-optimal operation. Note that the profile looks very similar to the one of case 1.1, the only noticeable difference is around the side draw stage. For case 4.2 the flow paths of components A and C are switched. See Table 2 for specifications.*

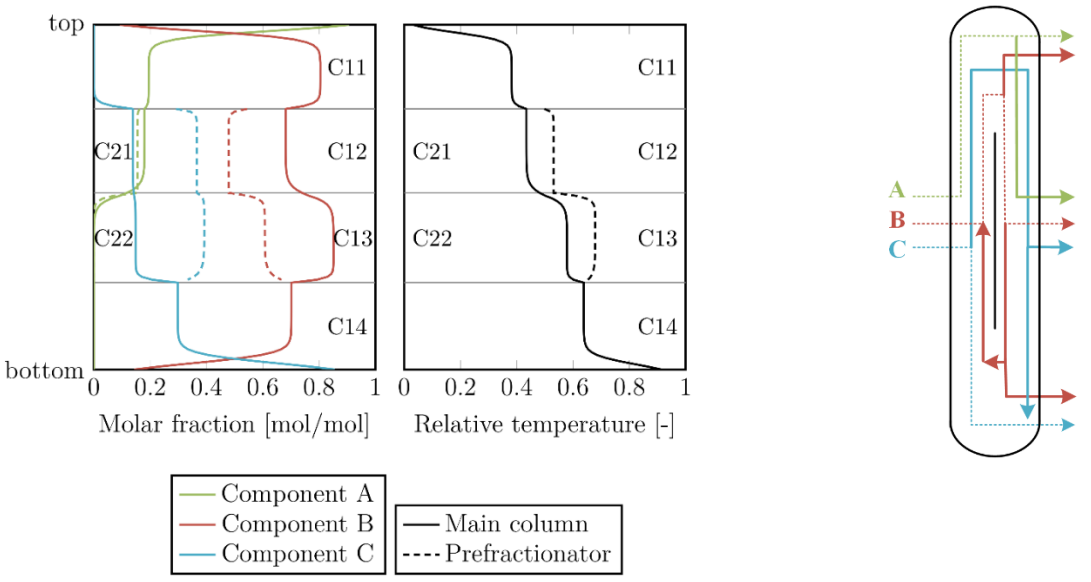

(a) (b)

Figure 17: Case 5.1. (a) Liquid composition and temperature profile and (b) net flow of components inside the column for non-optimal prefractionator operation providing $\dot{V}_{C14} = 1.08 \cdot \dot{V}_{\min}^{AB-C}$ *in the main column. Dotted lines show original optimal path of the components and solid lines represent different paths for non-optimal operation. For case is 5.2 the flow paths of components A and C are switched. See Table 2 for specifications.*

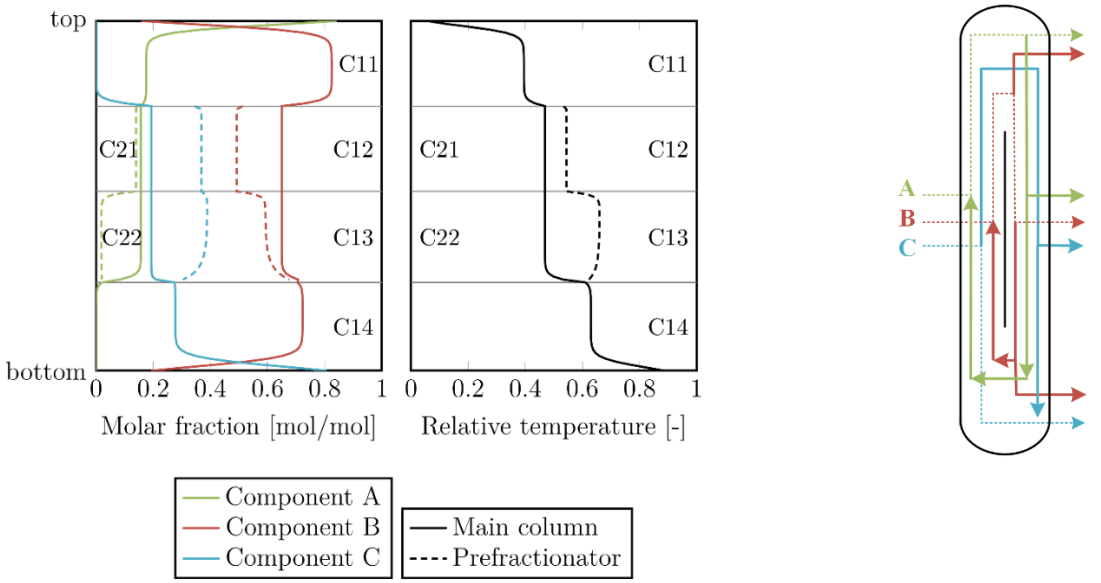

(a) (b)

Figure 18: Case 6. (a) Liquid composition and temperature profile and (b) net flow of components inside the column for non-optimal prefractionator operation providing $\dot{V}_{C14} = 1.08 \cdot \dot{V}_{\min}^{AB-C}$ *in the main column. Dotted lines show original optimal path of the components and solid lines represent different paths for non-optimal operation. See Table 2 for specifications.*

At the other side of the $\dot{V}_{min}$ boundaries (Figure 10), at low or negative $\dot{D}/\dot{F}$ ratios, the circulation is counterclockwise so it takes place from above the dividing wall. In case 4.2 only component B circulates. In case 5.2 component A starts to distribute between the prefractionator top and bottom product. Note that the corresponding profiles and net flow paths are not shown here, as they are a mirrored version of those in cases 4.1 and 5.2 (Figure 16 and Figure 17).

If the $\dot{D}/\dot{F}$ ratio is reduced further towards case 7, additionally component A starts to circulate around the top of the wall (Figure 19). In the most extreme case in case 8 even the heavy boiling component C circulates around the wall.

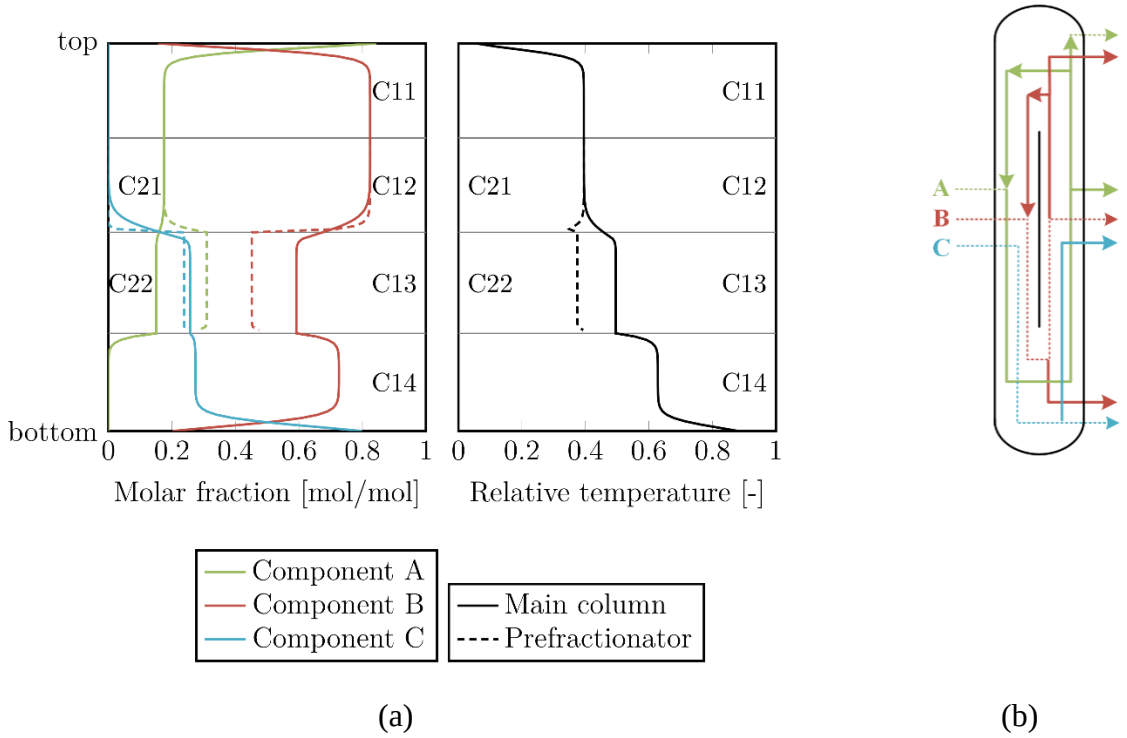

Figure 19: Case 7. (a) Liquid composition and temperature profile and (b) net flow of components inside the column for non-optimal prefractionator operation providing $\dot{V}_{C14} = 1.08 \cdot \dot{V}_{min}^{AB-C}$ in the main column. Dotted lines show original optimal path of the components and solid lines represent different paths for non-optimal operation. See Table 2 for specifications.

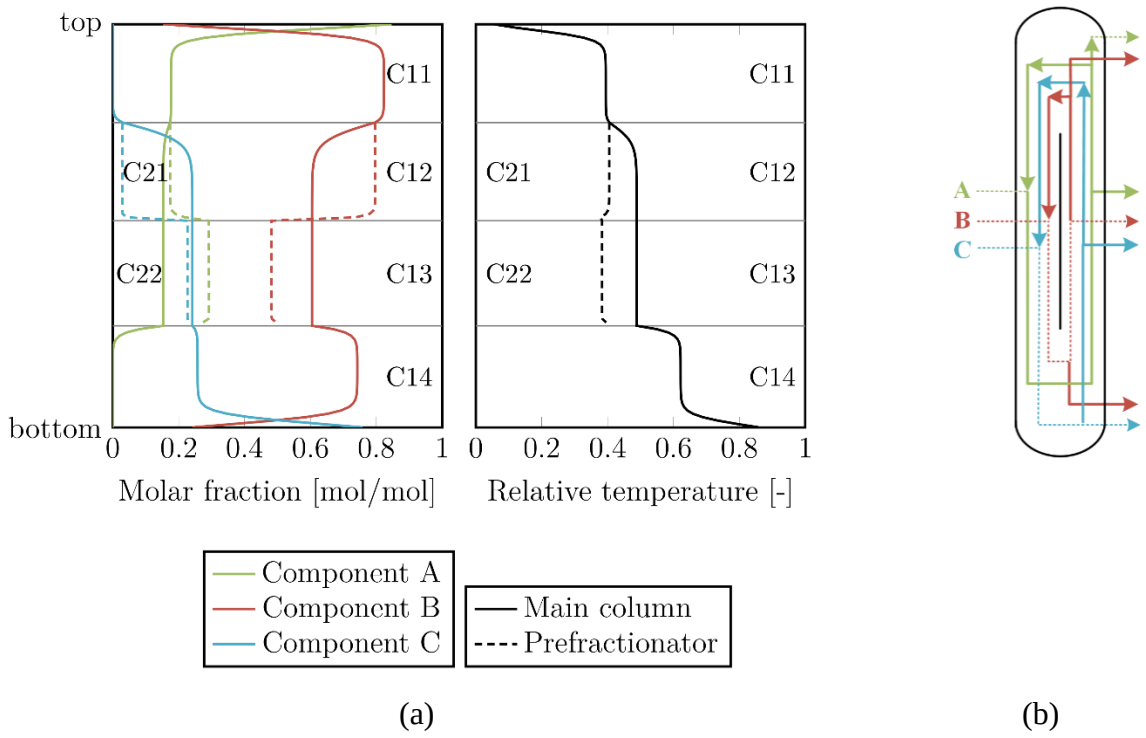

Figure 20: Case 8. (a) Liquid composition and temperature profile and (b) net flow of components inside the column for non-optimal prefractionator operation providing $\dot{V}_{C14} = 1.08 \cdot V_{\min}^{AB-C}$ *in the main column. Dotted lines show original optimal path of the components and solid lines represent different paths for non-optimal operation. See Table 2 for specifications.*

4.5 How to detect non-optimal prefractionator operation in temperature profile

In this Section the temperature profile of a prefractionator operation in the flexibility region is compared to different groups of non-optimal operations. Figure 21a compares the temperature profiles to those when the prefractionator is overpurified and correspondingly the main column is underpurified. Figure 21b compares the profiles to those with underpurification of the prefractionator. Figure 22 shows the profiles in cases with circulating components, with circulation around the upper part of the dividing wall in Figure 22a and below the dividing wall in Figure 22b.

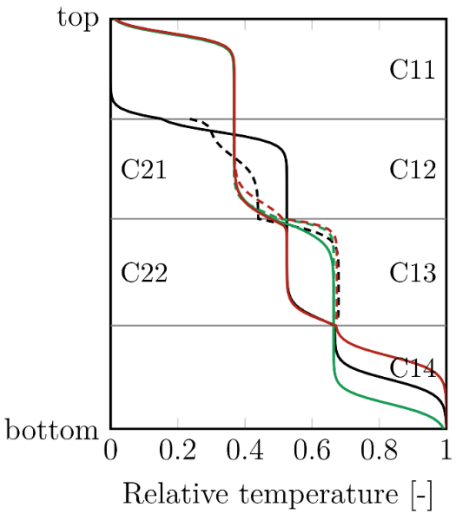

(a) Overpurified prefractionator (dashed lines), underpurified main column (solid lines)

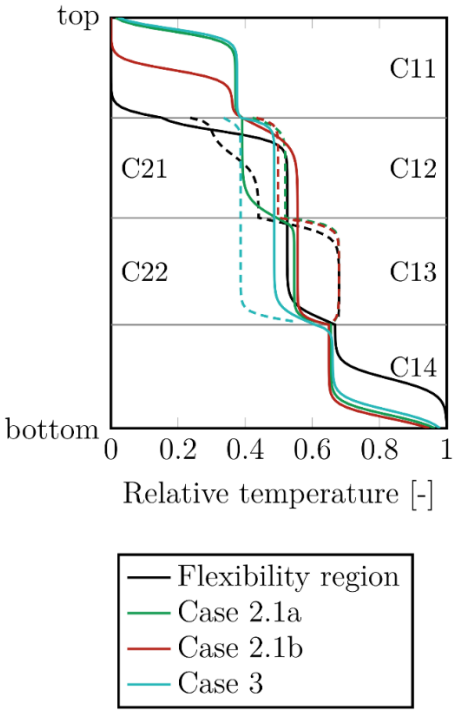

(b) Underpurified prefractionator (dashed lines) and underpurified main column (solid lines)

Figure 21: Temperature profiles of cases with over- and under-purification of prefractionator.

Based on the profiles and our recent publication about temperature profiles in distillation columns [27], relevant characteristics are concluded here.

Prefractionator:

- Three pinches in the prefractionator indicate an operation close to the $\dot{V}_{min}$ boundary between the A-BC and AB-C-maxima. Correspondingly, when operating in the flexibility region, there are also three pinches (or left-overs of these in terms of slope changes) visible. However, for a clear conclusion about whether the operation is inside or outside of the flexibility region, additionally the profile in the main column has to be evaluated.
- A continuous pinch above and below the feed stage in the prefractionator at the feed boiling point (between C21 and C22) without additional pinches means that all feed components

leave it at the top and bottom. This is a clear indication of underpurification (case 3) (Rules 4/5 from Table *1*).

Main column:

- A continuous pinch above and below the feed stage in the upper or lower main column (between sections C11+C12 and C13+C14) without additional pinches means that the main column is underpurified, in other words too little energy is provided. More energy input to the reboiler can solve this issue (but does not guarantee that the prefractionator is operated optimally also) (case 0, 1.1).
- A pinch in the middle of C11 without a pinch at the top end means that three components enter the upper main column and the heavy boiling component C disappears from the top product. Accordingly, the prefractionator is clearly not operated optimally (cases 2.1a, 3, 5.1, 6, 8).
- A pinch in the middle of C14 means that three components enter the lower main column and the light boiler disappears from the bottom product. Accordingly, the prefractionator is clearly not being operated optimally (cases 3, 6, 7, 8).

Whether components circulate or not is difficult to see from the temperature profiles (e.g., regions 2.1a and 5.1 are qualitatively very similar). However, another indication for assessing the operating point can be the temperature change in the prefractionator (between the top and bottom ends), which is shown for the case study simulations in combination with the resulting product purity of component B in the side product in Figure 23.

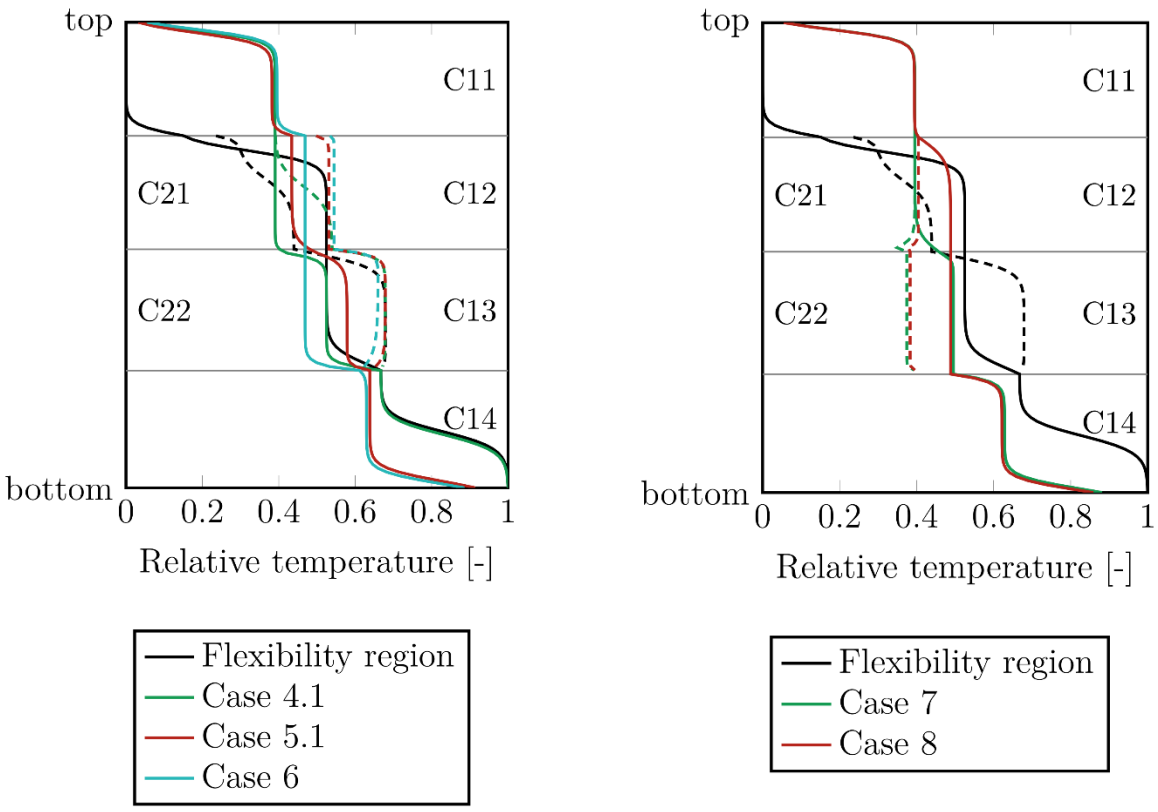

(a) Circulation above dividing wall (b) Circulation below dividing wall

Figure 22: Temperature profiles for cases with circulating components

The highest temperature change in the prefractionator is reached for operation within the flexibility region, which of course also leads to the highest purity. Non-optimal prefractionator operation leads on the one hand to lower purities and on the other hand also to a lower temperature change over the prefractionator, where the relationship is approximately linear. Interestingly, different slopes result for the scenarios with over- or under-purification of the prefractionator and those with circulating components. Very small or even negative temperature changes in the prefractionator are only found for scenarios with circulating components (cases 5.1, 5.2, 6, 7, 8). At a comparable temperature change, operation with circulating components (cases 4.1 and 4.2) results in lower purities than operation in those without (cases 0, 1.1, 1.2, 2.2a, 2.2b).

Note that these results are only an initial indication and further investigations are required to finally prove these findings. If they are found to be generally applicable this can be very useful to interpret the operation of a real plant. However, in any case preliminary simulations are needed to get a reference for the prefractionator temperature change in the optimal and non-optimal case.

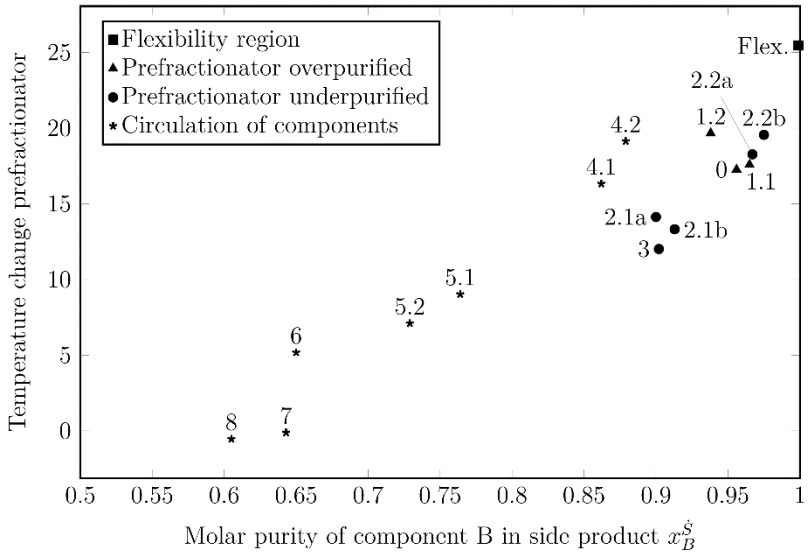

Figure 23: Temperature change in the prefractionator (from top to bottom end) resulting from operation in different cases

5 Generalization of results and further research suggestions

The results of this work are based on several assumptions, which includes the assumption of a ternary, equimolar and close to ideal mixture, fixed product flows equal to the feed flow of the corresponding target components and providing slightly more energy than the minimum demand in the main column and overall a high number of stages. If less stages are used, the energy demand increases. Nevertheless, in a previous publication it has been shown that the basic idea of the $\dot{V}_{\min}$ diagram can be extended to higher number of stages by merging it with an optimization or short-cut approach determining the energy demand for a finite number of stages [23]. Thus, it is assumed that the results from Figure 10 will still be valid but the peaks will be higher and the shape of the diagram may change based on the actual number of stages. Additionally, at lower number of stages pinches disappear, but they are still visible as a slope change in the temperature profile [27,28]. So generally, the authors believe that the results, including the flow patterns and usage of temperature profiles, are applicable for similar separation tasks in dividing wall columns. Additionally, several aspects need to be evaluated further in order to enable a comprehensive generalization of the results.

For mixtures with more than three components, it can be assumed that similar patterns exist, although the location of pinches in the profiles will change. Correspondingly, the interpretation of temperature profiles becomes more complex which may lower their usability to draw conclusions about the operation.

For less ideal mixtures, additional special behaviors, such as tangent pinches, can occur. This makes the interpretation of temperature profiles more difficult.

Further, the product flows are usually indirectly given by temperature controllers and are thus change during operation. With temperature control, it is usually possible to obtain at least a pure top or bottom product, but then some of the target components will be lost in the side draw, which will be impure. This will affect the temperature profiles, so the impact of changes in product flows on the profiles and flow patterns should be evaluated in more detail.

Note that the illustrated case represents the situation where the heavy/intermediate split (or the right-hand peak) sets the demand for the overall reboiler duty. There is a set of feed cases where the light/intermediate (or the leftmost peak) is limiting. Then, the optimality region will be mirrored to the other side of the preferred split point (on the branch in the $\dot{V}_{\min}$ diagram towards the highest peak). The same kind of analysis as shown in this paper can be carried out for that situation, but that is not included herein.

6 Summary and conclusions

Dividing wall columns are promising energy saving units for the chemical industry. However, to be able to exploit their full potential, every day and hour, the ability to identify and mitigate non-optimal operation is important. The results in this paper hopefully contribute to such understanding. The importance of the prefractionator operation on the overall performance of dividing wall columns was investigated in this work. It is already known that there is a certain operational flexibility regarding the vapor and liquid split ratios at the dividing wall. However, the authors are not aware of any publication focusing on what happens if the prefractionator is operated outside this range. This publication aims to close this gap and give an overview about possible scenarios. The reader should keep in mind that the results were obtained for a close to ideal BTX case study system at high number of stages.

First, the feasible operating range of the prefractionator is visualized in a $\dot{V}_{\min}$ diagram. As operation is moved off from the dividing wall column optimality region, (given by a line segment on the V-shape), the profiles and separation purity performance will change according to which region in the diagram the operation is moved into. The behaviour in each region is described in detail and this knowledge may be used to diagnose any given set of column profiles.

In the case study, 15 non-optimal prefractionator operation regions were identified. For each region, a certain type of internal flow pattern is observed which results in similar composition and temperature profiles. More generally, the cases can be classified into three groups: (a) overpurification of the prefractionator causing an underpurification of the main column (cases 0,

1.1, 1.2), (b) underpurification of the prefractionator and underpurification of main column (cases 2.1a, 2.1b, 2.2a, 2.2b, 3) and (c) operation with components circulating around the dividing wall (cases 4.1, 4.2, 5.1, 5.2, 6, 7, 8).

Additionally, it is shown how non-optimal operation can be detected based on the temperature profile in the column. These profiles can either be obtained from a flow sheet simulator or, if no internal sensors are available, by measuring the temperature of the outer shell of a real plant. In this regard keep in mind that other real-life effects like separation performance or maldistribution may affect the profiles, however these topics exceed the scope of this article. By comparing the profile of the given system with the profiles in this article, useful conclusions can be drawn. The obtained results indicate that the temperature change in the prefractionator may be a suitable parameter to detect non-optimal operation. The temperature change is higher when higher purities are obtained. However, more extensive studies should be performed, including using different mixtures, using different energy inputs to the main column and different product flows.

If a non-optimal prefractionator operation is detected, this can be counteracted by correcting the vapor and liquid splits. Usually, the liquid split can be manipulated during operation, while the vapor split results from the column design. To a certain extent the liquid split can be used to compensate a non-optimal vapor split, however, if the vapor flow is outside the flexibility range, the desired separation becomes infeasible.

Correspondingly, for a robust operation of dividing wall columns close to the energy minimum, also with regards to disturbances and changing feeds over the years, not only the liquid but also the vapor split ratio should be designed in a way that it can be manipulated. If not on-line, then at least to a changed fixed value if there is a known significant shift in feed properties.

7 Funding

Lena-Marie Ränger has been funded by the Deutsche Forschungsgemeinschaft (DFG, German Research Foundation) – Project number 504053756.

8 Symbols

8.1 Variables

Variable	Meaning
$\dot{B}$	Molar bottom product flow
$\dot{D}$	Molar top product (distillate) flow
$\dot{F}$	Molar feed flow
k	Number of components in feed stream
$\dot{L}$	Molar liquid flow
R	Split ratio at dividing wall (molar flow to prefractionator divided by total flow)
$\dot{S}$	Molar side draw flow
t	Relative Temperature
T	Temperature
$\dot{V}$	Molar vapor flow
w_i	Net flow of a component
x	Molar fraction in liquid phase
y	Molar fraction in vapor phase

8.2 Index

Index	Meaning
b	boiling
bot	column bottom
Cij	Column section numbering (see Figure 1a)
i	component, A, B, C
L	liquid

n	stage n
top	column top
max	upper limit
min	lower limit
V	vapor

9 References

[1] N. Asprion, G. Kaibel, Dividing wall columns: Fundamentals and recent advances, Chem. Eng. Process. Process Intensif. 49 (2010) 139–146. https://doi.org/10.1016/j.cep.2010.01.013.

[2] M.A. Schultz, D.G. Stewart, J.M. Harris, S.P. Rosenblum, M.S. Shakur, D.E. O'Brien, Reduce costs with dividing-wall columns, Chem. Eng. Prog. 98 (2002) 64–71.

[3] A. Kanda, R. Kalita, J.C. Gentry, Network of Dividing Wall Columns in Complex Process Units, Chemical Engineering Transactions 69 (2018).

[4] R. Premkumar, G.P. Rangaiah, Retrofitting conventional column systems to dividing-Wall Columns, Chem. Eng. Res. Des. 87 (2009) 47–60. https://doi.org/10.1016/j.cherd.2008.06.013.

[5] B. Slade, B. Stober, D. Simpson, Dividing Wall Column Revamp Optimizes Xylene Production, in: 2006 Spring Meet. 2nd Glob. Congr. Process Saf., 2006.

[6] A. Górak, Ž. Olujić, Distillation: Equipment and processes / edited by Andrzej Górak, Žarko Olujić, Academic Press, Amsterdam, 2014.

[7] I.J. Halvorsen, S. Skogestad, Optimal operation of Petlyuk distillation: Steady-state behavior, J. Process Control 9 (1999) 407–424. https://doi.org/10.1016/S0959-1524(99)00009-8.

[8] A.A. Kiss, Advanced distillation technologies: Design, control, and applications, First edition, Wiley, Chichester, West Sussex, United Kingdom, 2013. http://search.ebscohost.com/login.aspx?direct=true&scope=site&db=nlebk&db=nlabk&AN=566490.

[9] H.A. Kooijman, E. Sorensen, Recent advances and future perspectives on more sustainable and energy efficient distillation processes, Chem. Eng. Res. Des. 188 (2022) 473–482. https://doi.org/10.1016/j.cherd.2022.10.005.

[10] S. Jia, X. Qian, X. Yuan, Optimal design for dividing wall column using support vector machine and particle swarm optimization, Chem. Eng. Res. Des. 125 (2017) 422–432. https://doi.org/10.1016/j.cherd.2017.07.028.

[11] T. Waltermann, S. Sibbing, M. Skiborowski, Optimization-based design of dividing wall columns with extended and multiple dividing walls for three- and four-product separations, Chem. Eng. Process. Process Intensif. 146 (2019) 107688. https://doi.org/10.1016/j.cep.2019.107688.

[12] H. Benyounes, K. Benyahia, W. Shen, V. Gerbaud, L. Dong, S. Wei, Novel Procedure for Assessment of Feasible Design Parameters of Dividing-Wall Columns: Application to Non-azeotropic Mixtures, Ind. Eng. Chem. Res. 54 (2015) 5307–5318. https://doi.org/10.1021/ie5048576.

[13] J. Strandberg, Optimal operation of dividing wall columns, Doctoral thesis, Norwegian University of Science and Technology, 2011.
[14] I. Dejanović, L. Matijašević, Ž. Olujić, Dividing wall column—A breakthrough towards sustainable distilling, Chem. Eng. Process. Process Intensif. 49 (2010) 559–580. https://doi.org/10.1016/j.cep.2010.04.001.
[15] X. Ge, C. Ao, X. Yuan, Y. Luo, Investigation of the Effect of the Vapor Split Ratio Decision in Design on Operability for DWC by Numerical Simulation, Ind. Eng. Chem. Res. 53 (2014) 13383–13390. https://doi.org/10.1021/ie500686p.
[16] Lorenz Hilke-Marie, Staak Daniel, Grutzner Thomas, Repke Jens-Uwe, Divided wall columns: usefulness and challenges, Chem. Eng. Trans. 69 (2018) 229–234. https://doi.org/10.3303/CET1869039.
[17] A. Vazzoler, AN INTRODUCTION TO DIVIDING WALL COLUMNS DESIGN AND MODELLING (DWC), J. Eng. Res. 2 (2022) 2–27. https://doi.org/10.22533/at.ed.317222230014.
[18] I.J. Halvorsen, Minimum Energy Requirements in Complex Distillation Arrangements, Dr. ing. Thesis, Norwegian University of Science and Technology, 2001.
[19] I.J. Halvorsen, S. Skogestad, Minimum Energy Consumption in Multicomponent Distillation. 1. Vmin Diagram for a Two-Product Column, Ind. Eng. Chem. Res. 42 (2003) 596–604. https://doi.org/10.1021/ie010863g.
[20] I.J. Halvorsen, S. Skogestad, Minimum Energy Consumption in Multicomponent Distillation. 2. Three-Product Petlyuk Arrangements, Ind. Eng. Chem. Res. 42 (2003) 605–615. https://doi.org/10.1021/ie0108649.
[21] I.J. Halvorsen, S. Skogestad, Minimum Energy Consumption in Multicomponent Distillation. 3. More Than Three Products and Generalized Petlyuk Arrangements, Ind. Eng. Chem. Res. 42 (2003) 616–629. https://doi.org/10.1021/ie0108651.
[22] L.-M. Ränger, U. Preißinger, T. Grützner, Robust Initialization of Rigorous Process Simulations of Multiple Dividing Wall Columns via Vmin Diagrams, ChemEngineering 2 (2018) 25. https://doi.org/10.3390/chemengineering2020025.
[23] L.-M. Ränger, T. Grützner, Shortcut Method for Initialization of Dividing–Wall Columns and Estimating Pareto–Optimal NQ –Curves, Chem. Eng. Technol. 44 (2021) 1919–1928. https://doi.org/10.1002/ceat.202100256.
[24] C.J. King, Separation processes, second, McGraw Hill, NY, 1980.
[25] J. Stichlmair, H. Offers, R.W. Potthoff, Minimum reflux and minimum reboil in ternary distillation, Ind. Eng. Chem. Res. 32 (1993) 2438–2445. https://doi.org/10.1021/ie00022a029.
[26] A. Lucia, A. Amale, R. Taylor, Distillation pinch points and more, Comput. Chem. Eng. 32 (2008) 1342–1364. https://doi.org/10.1016/j.compchemeng.2007.06.019.
[27] L.-M. Ränger, I.J. Halvorsen, T. Grützner, S. Skogestad, Understanding Temperature Profiles of Distillation Columns, Ind. Eng. Chem. Res. 63 (2024) 4533–4546. https://doi.org/10.1021/acs.iecr.3c04102.
[28] L.-M. Ränger, I.J. Halvorsen, T. Grützner, S. Skogestad, Correction to “Understanding Temperature Profiles of Distillation Columns,” Ind. Eng. Chem. Res. (2024) acs.iecr.4c01893. https://doi.org/10.1021/acs.iecr.4c01893.
[29] L.-M. Ränger, Multi-Objective Optimization of Simple and Multiple Dividing Wall Columns and their Operational Flexibility Close to the Optimum, PhD Thesis, Universität Ulm, 2021. https://doi.org/10.18725/OPARU-40071.

912